

# Modelling the contribution of biogenic volatile organic compounds to new particle formation in the Jülich plant atmosphere chamber

P. Roldin<sup>1,2</sup>, L. Liao<sup>1</sup>, D. Mogensen<sup>1</sup>, M. Dal Maso<sup>3</sup>, A. Rusanen<sup>1</sup>, V.-M. Kerminen<sup>1</sup>, T. F. Mentel<sup>4</sup>, J. Wildt<sup>5</sup>, E. Kleist<sup>5</sup>, A. Kiendler-Scharr<sup>4</sup>, R. Tillmann<sup>4</sup>, M. Ehn<sup>1</sup>, M. Kulmala<sup>1</sup>, and M. Boy<sup>1</sup>

[1] {Department of Physics, University of Helsinki, P.O. Box 64, 00014 Helsinki, Finland}

[2] {Division of Nuclear Physics, Lund University, P.O. Box 118, 221 00 Lund, Sweden}

[3] {Department of Physics, Tampere University of Technology, P.O. Box 692, 33101 Tampere, Finland}

[4] {Institute for Energy- and Climate Research (IEK-8), Forschungszentrum Jülich, 52425 Jülich, Germany}

[5] {Institute of Biogeosciences (IBG-2), Forschungszentrum Jülich, 52425 Jülich, Germany}

Correspondence to: P. Roldin (pontus.roldin@nuclear.lu.se)

## Abstract

We used the Aerosol Dynamics gas- and particle-phase chemistry model for laboratory CHAMber studies (ADCHAM) to simulate the contribution of BVOC plant emissions to the observed new particle formation during photooxidation experiments performed in the Jülich Plant-Atmosphere Chamber. ADCHAM couples the detailed gas-phase chemistry from Master Chemical Mechanism with a novel aerosol dynamics and particle phase chemistry module. Our model simulations reveal that the observed particle growth either may have been controlled by the formation rate of semi- and low-volatility organic compounds in the gas-phase or by acid catalyzed heterogeneous reactions between semi-volatility organic compounds in the particle surface layer (e.g. peroxyhemiacetal dimer formation). The contribution of extremely low-volatility organic gas-phase compounds to the particle formation and growth was suppressed because of their rapid and irreversible wall losses. The

best correlation between the modelled and measured total particle number concentration ( $R^2 > 0.97$ ) was achieved if the nano-CN was formed by kinetic nucleation involving both sulphuric acid and BVOC oxidation products.

## 1 Introduction

New particle formation, including formation of nano condensation nuclei (nano-CN) (McMurry et al., 2011) and their growth to larger sizes, has been observed world-widely in continental boundary layers and free troposphere (Kulmala et al., 2004; Mirme et al., 2010). Field observations, laboratory experiments and model simulations indicate that gaseous sulphuric acid ( $H_2SO_4$ ) plays an important role in atmospheric nano-CN formation, yet  $H_2SO_4$  alone appears not to be able to explain all the steps of this process (Kulmala et al., 2000; Boy et al., 2003; Sipilä et al., 2010; Riipinen et al., 2007; Sihto et al., 2006; Kerminen et al., 2010; Kulmala et al., 2013, 2014). Basic compounds like ammonia and certain amines have been proposed to act as stabilizing compounds in nano-CN clusters (Berndt et al., 2010; Almeida et al., 2013; Kurtén et al., 2008), while subsequent steps of atmospheric new particle formation seem to rely on the presence of low-volatility organic compounds (LVOCs) (e.g., Metzger et al., 2010; Paasonen et al., 2010; Riipinen et al., 2012; Ehn et al., 2014; Schobesberger et al., 2013).

Oxidation products of biogenic volatile organic compounds (BVOCs) constitute the largest source of secondary organic aerosol (SOA) in the global atmosphere (Tsigaridis and Kanakidou, 2003; Hallquist et al., 2009; Spracklen et al., 2011), accounting for the main composition of SOA condensational growth (VanReken et al., 2006; Hao et al., 2009; Riipinen et al., 2012). BVOC oxidation also produces extremely low-volatility organic compounds (ELVOCs) essential to the new particle formation process in the atmosphere (Ehn et al., 2014). The most abundant group of BVOCs, accounting for more than half of their global emissions, are terpenoids (Guenther et al., 1995). Terpenoids include compounds consisting of one to several isoprene units, e.g. isoprene ( $C_5H_8$ ), monoterpenes ( $C_{10}H_{16}$ ), and sesquiterpenes ( $C_{15}H_{24}$ ). Oxidation products of monoterpenes have substantial contribution to SOA formation (Hoffmann et al., 1997, 1998; Laaksonen et al., 2008), and low-volatility substances produced by sesquiterpene-ozone reactions may also initiate SOA formation (Bonn and Moortgat, 2003). Oxidation of isoprene leads to the formation of SOA (Surratt et

al., 2006; Claeys et al., 2004), yet isoprene may also suppress the new particle formation process due to its high reactivity with OH (Kiendler-Scharr et al., 2009). Overall, the exact contribution of BVOCs to SOA still remains uncertain, especially with respect to the initial steps of atmospheric new particle formation.

In this study, we used the Aerosol Dynamics, gas- and particle-phase chemistry model for laboratory CHAMber studies (ADCHAM) (Roldin et al., 2014), to investigate the new particle formation during a measurement campaign conducted in the Jülich Plant Atmosphere Chamber (JPAC). The in-depth analysis of the chamber measurements is discussed in another paper (Dal Maso et al., 2014). Here, we use the full chamber dataset including gas and particle phase measurements, either as model input or to evaluate the modelled performance concerning the nano-CN formation and growth.

## 2 Measurement set up

The experiments were conducted in the JPAC located at Forschungszentrum Jülich, Germany. Detailed description regarding the chamber facility was given in previous articles (e.g., Mentel et al., 2009; Schimang et al., 2006). In addition, more details about this measurement campaign can be found from Dal Maso et al. (2014). In brief, the system consisted of two borosilicate glass chambers with PTFE Teflon floors. The chambers were operated as continuously stirred tank reactors (CSTR) with Teflon fans ensuring homogeneous air mixing. Each chamber housed adjustable temperature between 10 and 50 °C with a stability of  $\pm 0.5$  °C. The small chamber (1150 L) served as plant chamber and was connected to the larger chamber that worked as reaction chamber (1450 L, surface-area-to-volume ratio  $4.87 \text{ m}^{-1}$ ).

Three small trees aging from three to four years were brought from Hyytiälä, Finland, and included Scots pine (*Pinus sylvestris*), Norway spruce (*Picea abies*), and Silver birch (*Betula pendula*). These trees, representing the main boreal forest species in Finland, were placed in the JPAC plant chamber for almost two weeks before the intensive experiment campaign started. This allowed them to adjust to the chamber environment. Starting from the day when the trees were installed in the plant chamber, tree emissions were transferred into the reaction chamber, where O<sub>3</sub> was added together with water vapour directly and OH was generated periodically by turning on and off the UV light, in the same fashion as applied in the intensive

1 phase. New particles were formed every day during the UV-light on periods and gases and  
2 particles deposited on the chamber walls. Discharge lamps (Osram HQI 400 W/D) were used  
3 for illumination to simulate the solar light spectrum in both chambers. Filters (OptoChem,  
4 type IR3) that reflect wavelengths between 750 and 1050 nm were used as heat shields to  
5 avoid infrared radiation inflicted plant overheating (Fig. S1 in the supplementary material  
6 shows the measured light spectrum from the discharge lamps in the reaction chamber).

7 The ambient air was purified by an adsorption dryer (Zander, KEA 70) and a palladium  
8 catalyst (450 °C). O<sub>3</sub>, NO, NO<sub>2</sub> and VOC levels decreased significantly after passing the  
9 purification system. The flow through the plant chamber was 115 L min<sup>-1</sup> from which a  
10 fraction of 20 L min<sup>-1</sup> was transferred to the reaction chamber. This flow was kept nearly  
11 constant by keeping the pressure drop constant. In addition, the 10 L min<sup>-1</sup> flow containing  
12 ozone was added, controlled by a second flow controller.

13 The concentrations of O<sub>3</sub>, CO<sub>2</sub> and H<sub>2</sub>O were measured by commercial analytical instruments.  
14 Two Gas Chromatography Mass Spectrometer (GC-MS) systems were used, one to measure  
15 the VOC concentrations from C<sub>5</sub> to C<sub>20</sub> in the outflow air from the plant chamber (Heiden et  
16 al., 2003), and another to identify the OH concentration by determining the decrease in the  
17 concentration of 2-butanol in the reaction chamber (Kiendler-Scharr et al., 2009). Meanwhile,  
18 the VOC concentration was continuously measured by an on-line Proton Transfer Reaction  
19 Mass Spectrometer (PTR-MS) in the plant and reaction chamber. The gas phase H<sub>2</sub>SO<sub>4</sub>  
20 concentration in the reaction chamber was measured by a Chemical Ionization Mass  
21 Spectrometer (CIMS) (Petäjä et al., 2009; Mauldin et al., 1998). A prototype Airmodus  
22 Particle Size Magnifier (PSM) coupled with a TSI condensation particle counter (CPC) was  
23 used to count the total number concentration of particles larger than ca. 1.6 nm in diameter  
24 (Vanhanen et al., 2011) and a TSI CPC (TSI3022A) was used to measure the total  
25 concentration of particles larger than ca. 7 nm in diameter. A Scanning Mobility Particle Sizer  
26 (SMPS TSI3071 + TSI3025A) was used to measure the particle size distribution in the size  
27 range of 14 – 600 nm.

28 The real plant emissions and the simulated day and night conditions make these experiments  
29 suitable for evaluation of methods used to describe the atmospheric transformation (ageing) of  
30 BVOCs and SOA beyond the first gas-phase VOC oxidation stage (e.g. the 2-Dimensional  
31 Volatility Basis Set (2D-VBS) Donahue et al., 2011).

### 3 Description of the ADCHAM model and its application

ADCHAM is a model primarily developed for simulations of laboratory chamber experiments on SOA formation and ageing. The model includes modules for reversible partitioning of organic compounds to and from the chamber walls, all fundamental aerosol dynamics processes, detailed gas- and particle-phase chemistry and a kinetic multilayer model which can be used to simulate mass transfer limited mixing of compounds in the particle phase (Fig 1). Below we describe how ADCHAM was set up in this work. For a more detailed description of ADCHAM we refer to Roldin et al. (2014).

#### 3.1 Gas-phase chemistry

The gas-phase chemistry reactions were selected from the Master Chemical Mechanism (MCM) v3.2 (Jenkin et al., 1997, 2012; Saunders et al., 2003) via website: <http://mcm.leeds.ac.uk/MCM/>. The MCM is a near-explicit chemical degradation mechanism that simplifies the chemical path of compounds by lumping products beyond the second oxidation step. We used the Kinetic Pre-Processor (KPP) version 2.1 (Damian et al., 2002) to simulate the gas-phase chemistry.

Among all the compounds measured by GC-MS in the JPAC plant chamber, 28 organic compounds were included in the gas-phase chemistry mechanism (see Table 1). In the table, the “other MTs” equals to the concentration difference between the summation of the concentrations of the 13 selected monoterpenes by GC-MS and the total monoterpene concentration measured by PTR-MS, while the “other SQTs” equals to the summation of other sesquiterpene isomers besides the listed four sesquiterpenes measured by GC-MS. In total, the gas-phase chemistry mechanism includes 2294 species and 6487 chemical and photochemical reactions for the chemical calculations. This includes relevant inorganic reactions and the full chemistry path for isoprene,  $\alpha$ -pinene,  $\beta$ -pinene, limonene,  $\beta$ -caryophyllene, toluene, 2-butanol and hexanal. We also included the first-order reactions of OH, O<sub>3</sub>, and NO<sub>3</sub> with the following organic compounds: myrcene, sabinene, camphene, ocimene,  $\Delta^3$ -carene, “other MTs” (which assumed the same rate coefficients as  $\alpha$ -pinene), cineole (also known as eucalyptol), farnesene, “other SQTs” (which assumed the same rate coefficients as  $\beta$ -caryophyllene),  $\alpha$ -terpinene,  $\Delta$ -terpinene,  $\alpha$ -phellandrene,  $\beta$ -phellandrene, and terpinolene. Furthermore, we included the first-order reactions between OH and the following organic compounds: tricyclene, nonanal, and bornyl acetate. Finally, the first-order

reactions between O<sub>3</sub> and the following organic compounds were included:  $\alpha$ -humulene,  $\alpha$ -longipinene, and  $\Delta$ -cardinene were included.

Ocimene constituted a major fraction of MT on the first experiment day. The full chemistry path for ocimene is not available in MCM. However, we included its chemistry by approximating the chemistry beyond the first oxidation step with the chemistry path of limonene, for which the full MCM chemistry path is available. We also approximated the chemical path for  $\Delta^3$ -carene after the first oxidation step with that of  $\alpha$ -pinene, since both are bicyclic monoterpenes with an endocyclic double bond, as was done in Boy et al. (2013).

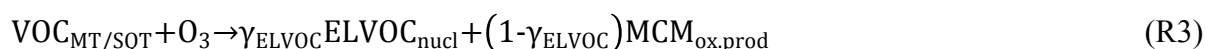
Based on the recent finding of rapid formation of extremely low-volatility organic compounds (ELVOCs) from ozonolysis of monoterpenes containing endocyclic double bonds (Ehn et al., 2014) we also included a simplified ELVOC formation mechanism in the MCM gas-phase chemistry code (R1), assuming that 7 mole % of the  $\alpha$ -pinene + O<sub>3</sub> and  $\Delta^3$ -carene + O<sub>3</sub> oxidation products were ELVOCs, with a molar mass of 325 g/mol and a vapour pressure of 10<sup>-10</sup> Pa, which approximately corresponds to the VBS bin of log<sub>10</sub>(C\*/ $\mu$ g m<sup>-3</sup>) = -5. We also performed simulations where we considered that ELVOCs was formed from ozonolysis of any monoterpene or sesquiterpene, with the same ELVOC molar yield as for  $\alpha$ -pinene. MCM<sub>ox.prod</sub> represents the MCMv3.2 oxidation products that was formed from the same reactions as the ELVOCs but via a different reaction pathway.



Ehn et al. (2014) also observed ELVOC formed from OH-oxidation of  $\alpha$ -pinene with an estimated maximum molar yield of 1 %. In this work we evaluated the potential contribution of ELVOCs formed from OH-oxidation by using an ELVOC molar yield of 1 % for any monoterpene and sesquiterpene that reacts with OH (R2).



In order to evaluate the potential influence of specific ELVOCs (e.g. dimers) which may be involved in the nano-CN formation (here denoted ELVOC<sub>nucl</sub>) we also included the possibility to add separate reactions where the monoterpene and sesquiterpene (VOC<sub>MT/SQT</sub>) that react with O<sub>3</sub> or OH form trace amounts of ELVOC<sub>nucl</sub> (R3-R4). In order to have little influence on the gas-phase chemistry or SOA formation, we used a very low ELVOC<sub>nucl</sub> yield ( $\gamma_{\text{ELVOC}}$ ) of 0.001 mole % and scaled the nucleation rate coefficient accordingly.





## 3.2 Aerosol dynamics

The aerosol dynamics module in ADCHAM is based on the aerosol dynamics code from the 2-D Lagrangian model for Aerosol Dynamics, gas-phase CHEMistry and radiative transfer (ADCHEM) (Roldin et al., 2011). It includes subroutines for nano-CN formation, condensation/evaporation, Brownian coagulation and particle deposition onto the chamber walls. ADCHAM simulates the condensation, dissolution and evaporation of sulphuric acid, ammonia, nitric acid, hydrochloric acid and an unlimited number of organic compounds using the analytic prediction of condensation scheme (Jacobson, 1997) and prediction of non-equilibrium growth scheme (Jacobson, 2005). The aerosol particle water content is calculated with a thermodynamics model (Sect 3.4).

ADCHAM considers the deposition of particles onto the chamber walls and keep track of the amount of deposited material on the walls. In Roldin et al. (2014) we kept track of each compound in each particle size bin that deposited on the chamber walls, and explicitly simulated the mass-transfer-limited gas-particle partitioning between the gas-phase and the wall deposited particles, assuming that the particles deposited on the walls remain as spherical particles on the walls. In this work, we instead assumed that the deposited SOA particles lose their individual particle identity and merge into the VOC wall matrix together with the gas-phase VOCs that deposit directly to the chamber walls (Sect. 3.5).

During the JPAC experiments the particles were formed by nucleation and, as a result of coagulation, wall losses and dilution, their average lifetime in the chamber was relatively short (less than 45 minutes, wherein dilution generally is the dominant loss process). Therefore, we expect that most of the formed particles were under charged with respect to the Boltzmann charge equilibrium distribution so that we do not have to consider the enhanced deposition rates induced by the particle charge (McMurry and Rader, 1985, Pierce et al., 2008 and Roldin et al., 2014). Thus, we calculated the first order wall deposition loss rate assuming that all particles were non-charged using the indoor deposition loss rate model from Lai and Nazaroff (2000), which accounts for different deposition loss rates on upward-, downward- and vertically facing surfaces. In the model by Lai and Nazaroff (2000) the fundamental (but unknown) parameter for the particle loss rate is the friction velocity,  $u^*$ . In this work we found that with a relatively small value of  $u^*$  ( $0.02 \text{ m s}^{-1}$ ), the model best captures the observed particle number and particle volume concentration loss rates after the

UV-light is turned off. With this value of  $u^*$  the deposition loss rate is equal to the observed ELVOC molecule loss rate measured by Ehn et al. (2014) when the particle (molecule) diameter is equal to 0.8 nm. We therefore used the value of  $u^* = 0.02 \text{ m s}^{-1}$  for all the model results presented in this work.

We evaluated six nano-CN formation parameterizations (Eq. 1-6) and compared them against base-case simulations with a fixed new-particle formation rate ( $J$ ). The first mechanism (Eq. 1) is sulphuric acid activation nucleation (Kulmala et al., 2006), Eq. 2 is used for kinetic nucleation of two  $\text{H}_2\text{SO}_4$  molecules (McMurry and Friedlander, 1979), Eq. 3 is used for kinetic nucleation of one  $\text{H}_2\text{SO}_4$  molecule and one  $\text{ELVOC}_{\text{nuc1}}$ , Eq. 4 is the nano-CN parameterization proposed by Riccobono et al., (2014) based on experiments in the CLOUD chamber, Eq. 5 represents a mechanism where single ELVOCs serve as nano-CN (Ehn et al., 2014), and Eq. 6 represent a kinetic type of nucleation mechanism with  $\text{ELVOC}_{\text{nuc1}}$ .

$$J = A[\text{H}_2\text{SO}_4] \quad (1)$$

$$J = K[\text{H}_2\text{SO}_4]^2 \quad (2)$$

$$J = K[\text{H}_2\text{SO}_4][\text{ELVOC}_{\text{nuc1}}] \quad (3)$$

$$J = K[\text{H}_2\text{SO}_4]^2[\text{ELVOC}_{\text{nuc1}}] \quad (4)$$

$$J = A[\text{ELVOC}_{\text{nuc1}}] \quad (5)$$

$$J = K[\text{ELVOC}_{\text{nuc1}}]^2 \quad (6)$$

$A \text{ (s}^{-1}\text{)}$  and  $K \text{ (cm}^3 \text{ s}^{-1}\text{)}$  in Eq 1-3 and Eq 5-6 are formation rate coefficients for activation type and kinetic type of nucleation, respectively. For Eq 4 the formation rate coefficient has the unit  $\text{cm}^6 \text{ s}^{-1}$ .

The composition of the nucleation clusters was chosen in order to match the respective new particle formation mechanism. The dry nano-CN volume was composed of equal mole fractions of  $\text{H}_2\text{SO}_4$  and  $\text{ELVOC}_{\text{nuc1}}$  when we used Eq 1, 3 or 5, equal mole fractions of  $\text{H}_2\text{SO}_4$  and  $\text{NH}_3$  when we used Eq. 2, and pure  $\text{ELVOC}_{\text{nuc1}}$  when we used Eq. 6. The molar mass of  $\text{ELVOC}_{\text{nuc1}}$  was assumed to be 500 g/mol. The equilibrium water content of the nano-CN clusters was calculated with the thermodynamics model. The dry particle size of the nano-CN was assumed to be 1.5 nm.

Both  $\text{ELVOC}_{\text{nuc1}}$  and  $\text{H}_2\text{SO}_4$  were assumed to be non-volatile. The  $\text{ELVOC}_{\text{nuc1}}$  first order wall loss rate was  $0.011 \text{ s}^{-1}$  according to Ehn et al. (2014). The  $\text{ELVOC}_{\text{nuc1}}$  condensation sink was



modelled explicitly with the condensation algorithm in ADCHAM. Chemical degradation of ELVOC<sub>nucl</sub> was not considered.

The ELVOC<sub>nucl</sub> involved in the nano-CN formation were assumed to be formed instantaneously after the first oxidation stage of monoterpenes and sesquiterpenes (R3-R4). With Eq. 3 and 4 we investigated six different sources of ELVOC<sub>nucl</sub>; (i) as a product formed exclusively from the ozonolysis of endocyclic monoterpenes ( $\alpha$ -pinene and  $\Delta^3$ -carene), (ii) from the ozonolysis of all monoterpene and sesquiterpene, (iii) from the ozonolysis of sesquiterpenes, (iv) from the OH and O<sub>3</sub> oxidation of monoterpenes and sesquiterpenes, (v) when monoterpenes and sesquiterpenes react with OH, or (vi) when sesquiterpenes react with O<sub>3</sub> or OH. When using Eqs. 5 and 6 we only considered the ELVOC<sub>nucl</sub> that was formed from monoterpenes and sesquiterpenes reacting with OH.

### 3.3 Size distribution structures

ADCHAM can be operated with the full-moving, fixed-sections or moving-centre particle size distribution approach (Roldin et al., 2011). In this work, we have tested both the fixed-sections approach and full-moving method using different numbers of size bins. The largest advantage of the full-moving approach compared to the fixed-sections approach is that it does not introduce any numerical diffusion problems and allows the particles to growth into their exact size during condensation. The main disadvantage is that new particle size bins need to be introduced when new particles are formed. In this work, we handled this by only introducing new particles formed by nucleation once every minute and at the same time as we added a new size bin for the freshly nucleated particles, we also removed the size bin containing the largest (oldest) particles. In order to not remove any particles within a time frame substantially longer than their average residence time in the reaction chamber, which was about 45 minutes, we used 400 size bins for the full-moving approach. Thus, with this method we kept track of the nucleated particles for 400 minutes (almost 9 times the average residence time in the chamber), before they were removed from the modelled size distribution. This method was compared with the fixed-section approach using a different number of size bins in the diameter ( $D_p$ ) range 1.5 to 800 nm. Based on these tests we could conclude that the fixed-section approach was not suitable due to numerical diffusion if the number of size bins were less than 400 (Fig. S2 in the supplementary material). With the full-moving approach the particle volume (PV) and particle number concentrations (PN) were well conserved although the last size bin was removed once every minute (Fig. S3).

Therefore, we decided to use the full-moving method to represent the particle number size distribution in this work.

One difficulty with the full-moving method is that the particle number size distribution needs to be mapped back onto a fixed diameter grid in order to illustrate it as a  $dPN/d\log D_p$  distribution. This grid needs to be relatively coarse in order to not get a “jumpy” graphical representation of the particle number size distribution. For this we used 50 size bins between 1.5 and 360 nm in diameter.

### 3.4 Particle phase chemistry and phase-state

ADCHAM includes a detailed particle-phase chemistry module, which is used to calculate the particle equilibrium water content, the particle acidity, nitric acid and hydrochloric acid saturation vapour pressures for each particle size bin, and the non-ideal interactions between organic compounds, water and inorganic ions using the activity coefficient model AIOMFAC (Zuend et al., 2008, 2011). In this work, we did not model the specific interactions between the organic and inorganic compounds but assumed a complete phase-separation of the inorganic- and organic particle phase. We used AIOMFAC to calculate the equilibrium water content in both the inorganic and organic particle phase and the individual compound activity coefficients. The organic compound activity coefficients were used when deriving the organic compounds saturation vapour pressures above each particle size (Sect. 3.6).

The particle phase chemistry module also contains subroutines that can be used to calculate organic salt formation, oligomerization and heterogeneous oxidation (Roldin et al., 2014). Recently, Shiraiwa et al. (2013) illustrated what peroxyhemiacetal (PHA) formation between organic compounds containing aldehydes and hydroperoxide functional groups may proceed fast and contribute to a large and rapid increase of the formed SOA mass during photooxidation experiments. In this work we evaluate if this type of heterogeneous dimer formation mechanism may explain the observed nano-particle growth during the JPAC experiment. For this we tested to use a constant value of the PHA formation rate ( $k_{PHA}$ ) of  $12 \text{ M}^{-1} \text{ s}^{-1}$  adopted from Shiraiwa et al. (2013). We also tested to model  $k_{PHA}$  as a parameterization of the sulphate particle mole concentration ( $x_{S(VI)}$ ), assuming that the PHA formation is acid catalysed by the co-condensing  $\text{H}_2\text{SO}_4$  (Eq 7).

$$k_{PHA} = B \cdot x_{S(VI)} \text{ (M}^{-1}\text{s}^{-1}\text{)} \quad (7)$$

Here  $B$  is a constant, the value of which we varied in the range  $1\text{-}500 \text{ M}^{-1} \text{ s}^{-1}$ .

In this work we used the kinetic-multi-layer module in ADCHAM for investigating weather the phase-state of the SOA particles might have influenced the evolution of the particle number size distribution. In order to do this, we divided each particle into three layers (an approximately monolayer thick surface layer of 0.7 nm, and two bulk-layers). We considered the two extreme conditions where the SOA particles either were considered to be completely liquid-like (no concentration difference between the surface and bulk layers) or solid-like (no molecule transport between the surface and the particle bulk layers). Still, this had only a minor effect on the modelled particle growth (SOA formation), but by treating the SOA as solid-like improved the agreement between the modelled and measured SOA particle volume decay when the UV-light was turned off (Fig. S4). Thus, for the simulations used to produce the results presented in Sect 4 we treated the SOA particles as solid-like with the assumption that the molecule transport between the particle bulk and the particle surface-layer is relatively slow compared to the time scale it takes for the condensation to form a new monolayer thick surface layer.

### 3.5 Reversible VOC wall loss

The JPAC reaction chamber was mixed with a Teflon fan with mixing times <2 min. The first order VOC wall loss rate to the chamber walls ( $k_w$ ) was therefore governed by the molecular diffusion across the boundary layer near the chamber walls and by the uptake rate at the wall surface. According to McMurry and Grosjean (1985), the first order VOC wall loss rate for FEP Teflon films ( $k_{w,FEP}$ ) can be modelled with Eq. 8, which has two key parameters; the VOC wall mass accommodation coefficient ( $\alpha_w$ ) and the coefficient of eddy diffusion ( $k_e$ ). Unfortunately neither  $\alpha_w$  or  $k_e$  can be derived easily. Based on the observed wall losses of particles, McMurry and Radar (1985) estimated  $k_e$  to be  $0.12 \text{ s}^{-1}$  in a  $60 \text{ m}^3$  FEP Teflon film chamber. Zhang et al. (2015) estimated  $k_e$  to be  $0.075 \text{ s}^{-1}$  and  $0.015 \text{ s}^{-1}$  in two not actively mixed FEP Teflon film chambers with volumes of 24 and  $28 \text{ m}^3$ .

$$k_{w,FEP} = \frac{A_w}{V_{chamber}} \left( \frac{\alpha_w \bar{v} / 4}{1 + (\frac{\pi}{2}) \alpha_w \bar{v} / (4 \sqrt{k_e D})} \right) \quad (8)$$

Here  $A_w$  is the chamber wall surface area,  $V_{chamber}$  is the chamber volume,  $\bar{v}$  is the mean thermal speed of the gas molecules and  $D$  is the molecular diffusion coefficient.

In the JPAC reaction chamber Ehn et al. (2014) observed ELVOC first order wall loss rates in the range  $0.013\text{-}0.011 \text{ s}^{-1}$ . By inserting a value of  $0.011 \text{ s}^{-1}$  for  $k_{w,FEP}$  in Eq. 8 and assuming that the surface wall uptake rate is not limiting the ELVOC wall loss rate ( $\alpha_w > 10^{-3}$ ) we get a

$k_e$  of  $4.2 \text{ s}^{-1}$  for the JPAC reaction chamber. This value is substantially larger than what was estimated by Zhang et al. (2015) and McMurry and Radar (1985) and is probably because the JPAC reaction chamber was actively mixed and has a smaller volume.

From measurements in a  $4 \text{ m}^3$  FEP Teflon chamber Kokkola et al. (2014) observed that for nopinone which has a pure-liquid saturation vapour pressure ( $p_0$ ) of 53 Pa, the gas-wall equilibrium was reached within a few minutes and  $k_{w,\text{FEP}}$  was  $\geq 0.03 \text{ s}^{-1}$ . The observations by Ehn et al. (2014) and Kokkola et al. (2014) indicate that gas-wall equilibration can be reached rapidly for both volatile and low volatile VOCs and that their uptake on the chamber walls is primarily limited by the transport to the chamber walls and not by surface uptake ( $\alpha_w$ ). In contrast, Zhang et al. (2014) observed that the gas-phase concentration of 25 different oxidized VOCs ( $p_0 = 6 \times 10^{-6} - 20 \text{ Pa}$ ) slowly decreased over more than 18 hours without reaching gas-wall equilibrium. These experiments were performed in a  $24 \text{ m}^3$  FEP Teflon film chamber that was not actively mixed. Based on Eq. 8, Zhang et al. (2014) concluded that the VOC wall loss rate onto the FEB Teflon film walls was primarily limited by the surface uptake ( $\alpha_w$ ) and not by the molecule diffusion to the chamber walls. Zhang et al., (2014) also derived a parameterization of  $\alpha_w$  as a function of the compounds pure liquid saturation vapour pressure.

Based on the rapid ELVOC wall losses observed by Ehn et al. (2014), we assumed that the VOC losses to the JPAC reaction chamber walls was primarily governed by the molecule diffusion to the chamber walls and used a constant  $k_w$  equal to  $0.011 \text{ s}^{-1}$  for all condensable organic compounds. However, we also performed test simulations using Eq 8 and the  $\alpha_w$  parameterization from Zhang et al. (2014).

According to Matsunaga and Ziemann (2010) the loss rate of VOCs from FEP Teflon chamber walls back to the gas-phase ( $k_g \text{ (s}^{-1}\text{)})$  can be represented by Eq 9,

$$k_{g,i} = \frac{k_w}{(RT/p_{0,i}C_w/\gamma_{w,i})} \quad (9)$$

where  $C_w$  in Eq 9 is an effective mole concentration of organic compounds on the chamber walls ( $\text{mol m}^{-3}$ ) and  $\gamma_{w,i}$  is the activity coefficient of compounds  $i$  in the organic film on the chamber walls,  $T$  is the temperature in Kelvin and  $R$  is the universal gas constant ( $\text{J mol}^{-1} \text{ K}^{-1}$ ). According to Matsunaga and Ziemann (2010), the FEP Teflon film walls serve as a large organic pool where VOCs can absorb ( $C_w/\gamma_{w,i}$  on the order of  $100 \mu\text{mol m}^{-3}$ ). Thus, the actual VOCs deposited on the chamber walls is considered to have a negligible contribution to  $C_w$ .

We assumed that there was practically no  $C_w$  on the glass for the VOCs to dissolve into. We also estimated that even if the deposited VOCs and SOA were distributed as a molecule monolayer on the walls, the VOCs formed during the simulated experiment could only cover maximum 2 % of the total glass wall surface area in the end of the measurement campaign (see supplementary material). Thus, we assumed that the VOC losses onto the glass wall surfaces could be treated as a condensation process but without dissolution (absorption) into an organic matrix on the walls. With this approach the uptake of compound  $i$  is governed by the difference between the concentration in the gas-phase ( $c_{g,i}$ ) and the pure liquid saturation concentration ( $c_{0,i}$ ) (Eq 10-11). Thus, as long as  $c_{g,i} < c_{0,i}$  the VOC will not condense on the glass walls. For many of the semi-volatility organic compounds (SVOCs), the limit at which  $c_{g,i}$  become larger than  $c_{0,i}$  was never reached during the experiments.

$$\frac{dc_{g,i}}{dt} = -k_w(c_{g,i} - c_{0,i}) \quad (\text{if } c_{g,i} > c_{0,i} \text{ or if } c_{w,i} > 0) \quad (10)$$

$$\frac{dc_{w,i}}{dt} = k_w(c_{g,i} - c_{0,i}) \quad (11)$$

For the PTFE Teflon floor, we used the theory developed for FEP Teflon films (Eq. 9, 12 and 13), assuming that the PTFE Teflon surface (in total 15 % of the total chamber surface area) has a  $C_w/\gamma_{w,i} = 100 \mu\text{mol m}^{-3}$  and  $k_{w,i} = 1.7 \times 10^{-3} \text{ s}^{-1}$  ( $0.15 \times 0.011 \text{ s}^{-1}$ ).

$$\frac{dc_{g,i}}{dt} = -k_{w,i}c_{g,i} + k_{g,i}c_{w,i} \quad (12)$$

$$\frac{dc_{w,i}}{dt} = k_{w,i}c_{g,i} - k_{g,i}c_{w,i} \quad (13)$$

In order to mimic the actual experiment procedure (Sect 2), we started the model simulations by running ADCHAM 14 days prior to the actual experiments started, with conditions similar to Day 1 of the experiment campaign (see Sect 3.7). This allowed the VOC concentration to build up on the chamber walls.

### 3.6 Condensable organic compound properties

In this work, we used two different approaches to simulate the SOA formation. In the first, the SOA formation was modelled by considering the gas-particle partitioning of all non-radical organic compounds from the MCMv3.2 gas-phase chemistry code with estimated pure-liquid saturation vapour pressure lower than  $10^{-2} \text{ Pa}$  at  $T=289 \text{ K}$  (in total 488 compounds). The pure-liquid saturation vapour pressures of these compounds were estimated using the boiling point and vapour pressure extrapolation method from Nannoolal et al. (2004; 2008), here after

referred to as the Nannool method. MCMv3.2 only includes one sesquiterpene:  $\beta$ -caryophyllene. As an attempt to take into account the SOA formation from the other sesquiterpens, for these simulations all sesquiterpenes were treated as  $\beta$ -caryophyllene.

The second method is the 2D-VBS approach (Jimenez et al., 2009; Donahue et al., 2011), which is a simplified approach to describe how the volatility distribution of the VOCs (as a function of their Oxygen to Carbon ratio (O:C)) evolves beyond the first oxidation step. A detailed description of the structure and general assumptions of the 2D-VBS method used in ADCHAM is given by Hermansson et al. (2014). Here we primarily describe how the 2D-VBS was modified in order to better capture the SOA formation observed during the JPAC experiments.

The 2D-VBS compounds were distributed across 11 volatility classes separated by powers of 10 in saturation concentration (at the standard temperature 298 K ( $C_{298}^*$ )), ranging from  $10^{-7}$  to  $10^3 \mu\text{g m}^{-3}$ , and 12 discrete O:C from 0.1 to 1.2, in steps of 0.1. VOCs were introduced into the 2D-VBS by scaling the amount of reacted monoterpenes and sesquiterpenes with stoichiometric VBS yield parameterizations that represent the volatility distribution of the first generation oxidation products. We used the parameterizations from Table 3 in Henry et al. (2012). These parameterizations represent the first generation product volatility distributions formed during experiments where  $\alpha$ -pinene was primarily oxidized by ozone (no OH-scavenger) or where  $\alpha$ -pinene was oxidized by OH. We used the former parameterization to represent the first generation terpene (monoterpenes and sesquiterpenes) oxidation products during the UV-off periods and the later for the UV-light on periods. ELVOCs formed as first generation oxidation products from R1 were introduced into the 2D-VBS assuming that they had a O:C of 1 and  $C_{298}^* = 10^{-7} \mu\text{g m}^{-3}$ .

Hermansson et al. (2014) illustrated that the modelled SOA formation is sensitive to the volatility distribution and the assumed O:C of the first generation oxidation products. Moreover it depends on how the functionalization and fragmentation pattern is represented in the VBS and the reaction rate constant between the VOCs and OH. Equation 14 from Jimenez et al. (2009) was used to represent how the fraction of VOCs which fragmentize upon oxidation varies as a function of their O:C.

$$f_{\text{frag}} = (\text{O:C})^y \quad (14)$$

Jimenez et al. (2009) assumed that  $y$  was equal to  $1/6$ , that the 2D-VBS compounds were

oxidized by OH with a reaction rate coefficient ( $k_{OH}$ ) of  $3 \times 10^{-11} \text{ cm}^3 \text{ s}^{-1}$ , and that the compounds that fragmentize had equal probabilities to split at any of the carbon bonds. However, with this 2D-VBS setup, ADCHAM substantially overestimated the SOA formation (Fig. S5). This was mainly because a substantial fraction of the 2D-VBS fragmentation products were still less volatile than the reacting VOCs. If we instead assumed that all fragmenting compounds (on a mole fraction basis with equal proportions) end up into the VBS bins where  $C_{298}^*$  is at least 3 order of magnitude larger than the corresponding functionalization products, and decreased the probability of fragmentation somewhat ( $y=1/3$ ), the modelled particle volume concentration agreed better with the measurements (Fig. S6). Thus, in the proceeding sections we used this fragmentation parameterization. We also performed sensitivity tests where we varied the value of  $k_{OH}$  in the range of  $3 \times 10^{-11}$  to  $5 \times 10^{-11} \text{ cm}^3 \text{ s}^{-1}$  and the O:C of the first generation oxidation products in the range of 0.3 to 0.5 (Fig. S6). Based on these tests, we decided to use the values of  $k_{OH} = 5 \times 10^{-11} \text{ cm}^3 \text{ s}^{-1}$  and O:C = 0.4 for the first generation oxidation products in the simulations used to produce the results in Sect. 4.

The temperature dependence of the 2D-VBS saturation concentrations were derived using the Clausius Clapeyron equation and assuming the following form for the heat of vaporization ( $\Delta H$ ; Epstein et al., 2010):

$$\Delta H = -11 \times \log_{10} C_{300}^* + 129 \text{ kJ mol}^{-1} \quad (15)$$

Both with the 2D-VBS and when the MCM compounds were used to represent the condensable organic compounds, the Raoult's law and the Kelvin equation were used to calculate the saturation vapour pressure ( $p_{s,i,j}$ ) for each compound ( $i$ ) above each particle size ( $j$ ) (Eq 16). With the 2D-VBS we assumed that the organic compounds were mixed ideally (unity activity coefficients ( $\gamma_i$ )). However, for the MCM compounds the molecule structure is known, so we calculated the organic compound activity coefficients in the SOA particle mixtures using AIOMFAC.

$$p_{s,i,j} = p_{0,i} x_{i,j} \gamma_{i,j} e^{\left( \frac{4M_i \sigma_i}{RT \rho_j D_{p,j}} \right)} \quad (16)$$

where  $x_{i,j}$  is the mole fraction of compound  $i$  in the particle surface layer of particles in size bin  $j$ ,  $M_i$  is the molar mass of compound  $i$  and  $\rho$  is the density of the absorbing phase. In this work the surface tension of the organic compounds ( $\sigma_i$ ) was estimated to be equal to 0.05 N

$\text{m}^{-1}$  following Riipinen et al. (2010), even though we also tested the values of  $\sigma_i$  in the range 0.02 to  $0.07 \text{ N m}^{-1}$ . These sensitivity tests revealed that the modelled total particle number concentration decreased by approximately 10 % and the total particle volume concentration by approximately 30 % when the value of  $\sigma_i$  was increased from 0.02 to  $0.07 \text{ N m}^{-1}$  (Fig. S7).

### 3.7 Optimizing model input parameters

We used the ADCHAM model to simulate the new particle formation and growth during one measurement campaign conducted in the JPAC chamber. We chose to study the first four continuous days from the measurement campaign because these days had continuous measurements, coverage of the dataset was complete and UV light-on period was the same.

The measured temperature and relative humidity (RH) in the JPAC reaction chamber were used directly in the model as input. The values from the first four days are illustrated in Fig. 2.

The purple bars in the figures illustrate the UV-on periods. The temperature stabilized around noon on Day-1, after that the temperature was ca.  $16^\circ\text{C}$  for all days. The RH had minor fluctuations during the experiment. RH was kept to ca. 60% during UV-on periods for the first three days. On Day-4, the RH was around 55 %. In addition, 8 discharge lamps were used to simulate solar illumination on Day-1 in the plant chamber, but only 4 lamps were used on the remaining days to generate lower levels of VOC emissions from the trees.

Because the inflow of ambient air into the JPAC chamber was purified by an adsorption dryer, by default, the concentrations of  $\text{NO}$ ,  $\text{NO}_2$ ,  $\text{SO}_2$ , and  $\text{CO}$  in the inflow to the reaction chamber were assumed to be 0.03, 0.2, 0.015 and 15 ppbv, respectively. However, in order to evaluate how sensitive the model results was, in particular the modelled VOC composition and SOA formation, we also performed sensitivity tests where we varied the inflow concentrations of  $\text{NO}_x$  ( $\text{NO} + \text{NO}_2$ ) within the range of 0.05-1 ppbv. Concentrations of VOCs in the inflow to the reaction chamber were based on the GC-MS and PTR-MS data. The initial concentrations of all VOCs were set to zero. The measured concentrations of isoprene, monoterpenes and sesquiterpenes (in the plant chamber) are illustrated in Fig. 3. The monoterpene and sesquiterpene concentrations displayed a certain diurnal distribution pattern, because the discharge lamps mimicked sunlight in the plant chamber. The total monoterpene concentration exceeded 4 ppbv on Day-1, and then decreased to a value below 2 ppbv on the following three days. In particular, the ocimene concentration was the highest on Day-1, which can be explained by the fact that ocimene emission is light dependent (Owen et al., 2002), and the simulated solar light intensity in the plant chamber from the discharge lamps



was two times higher on Day-1 than during Day 2-4.

The isoprene concentration and the total sesquiterpene concentration were about an order of magnitude lower than the monoterpene concentration. Overall, the measured concentrations of terpenes were at similar levels as ambient air concentrations in boreal forest environments (Ruuskanen et al., 2009).

At the first attempt, we tried to simulate the O<sub>3</sub> and OH concentrations with the gas-phase chemistry mechanism. An OH sink has been determined in the empty chamber by direct OH-LIF measurements (Diss. Sebastian Broch) and has been always found to be within 2 - 4 s<sup>-1</sup>. However, even with this OH sink, the model could not capture the observed gradual decrease in the O<sub>3</sub> concentration and increase in OH concentration during the UV-light on periods without either varying the UV-light intensity or the OH sink.

Therefore, we decided to use the measured O<sub>3</sub> and H<sub>2</sub>SO<sub>4</sub> concentrations, and estimated OH concentration, as input to the model. Figure 4a shows the measured O<sub>3</sub> concentration during the experiment, Fig. 4b shows the estimated OH concentration based on the observed loss rate of 2-butanol and Fig. 4c shows the measured H<sub>2</sub>SO<sub>4</sub> concentration. When the UV-light was turned on the H<sub>2</sub>SO<sub>4</sub> concentration increased very rapidly and had a distinct peak. This is most likely due to an initial peak in the OH concentration at the moment when the UV-lamps was turned on. In the model we represented this by setting the OH concentration to 5×10<sup>7</sup> molecules cm<sup>-3</sup> for the 12 first minutes after the UV-light were turned on.

The photolysis rates were simulated using the quantum yields and absorption cross sections reported at the MCMv3.2 web site. The light spectrum in the reaction chamber was estimated using the measured spectrum for the discharge lamps in the wavelength range 280-650 nm (Fig. S1) and with a single UV-light peak at a wavelength of 254 nm, which represents the UV-spectrum from the Philips, TUV 40W lamp. The UV-light source intensity corresponds to a O(<sup>1</sup>D) photolysis rate of 2.9×10<sup>-3</sup> s<sup>-1</sup> (Mentel et al., 2009). In order to evaluate the potential influence of the 254 nm wavelength UV-light on the VOC composition and SOA formation we performed a model simulation where the 254 nm UV-light was not considered when calculating the photolysis rates. This test showed that the modelled condensable organic composition and the SOA formation were not noticeable influenced by the 254 nm UV-light source.

## 4 Results and discussion

Table 2 summarizes the different model tests that we performed in this work in order to constrain the VOC wall losses, the aerosol dynamics-, gas- and particle-phase chemistry mechanisms that can explain the nano-CN formation and growth observed during the JPAC experiments presented in Sect 2.

### 4.1 Time series of BVOC concentrations

To investigate the potential contribution of BVOCs to the nano-CN formation and growth, it is essential to properly predict the time series of the BVOC concentrations. The modelled isoprene, monoterpene, and sesquiterpene concentrations in the JPAC reaction chamber are plotted in Fig. 5, together with isoprene and total monoterpene concentrations measured by the PTR-MS. The modelled isoprene concentrations were in a good agreement with the measurements during the UV-off period on Day-1. During the rest of the simulated four days period, the simulated isoprene concentration was generally lower than the observations. However, considering the low isoprene concentrations and the uncertainties in the PTR-MS measurements, we cannot draw any conclusions on whether the model actually underestimates the isoprene concentration or not.

The summation of the modelled monoterpene isomer concentrations reached the same level as the measurements. During the dark periods, the monoterpene concentrations in the reaction chamber decreased to about one third of their concentrations measured in the plant chamber. This was because of the in-flow dilution and chemical reactions with  $O_3$ . When the UV light was switched on, the monoterpene concentration decreased sharply due to OH oxidation, as seen both from the measurements and simulation results in Fig. 5. Before the UV-lights were turned on ~80 % of the reacting monoterpenes were oxidized by  $O_3$ . At the UV onset this number dropped to ~10 % and in the end of the UV-on periods only ~2 % of the oxidized monoterpenes were oxidized by  $O_3$ . The modelled monoterpene concentration shows a somewhat more pronounced decrease during the UV-on periods than measurement. However, as with the isoprene concentration, the relative uncertainties in the PTR-MS measurements increases at lower concentrations and part of the PTR-MS unity resolution mass peak that was interpreted as monoterpenes may also have had small contributions from other VOCs.

The sesquiterpene concentrations were below the detection limit of the PTR-MS. Our

modelled results show that the sesquiterpenes were strongly oxidized by  $O_3$  once the tree emission from the plant chamber entered the reaction chamber (Fig. 3). Even when the UV-lights were turned on, 40 to 60 % of the sesquiterpenes were oxidized by  $O_3$  and the rest by OH. The sesquiterpene concentrations decreased rapidly to below 0.01 ppbv. In addition, the sesquiterpene concentrations showed a minor decrease during UV-on periods because of the oxidation by OH.

Although a large fraction of the monoterpenes and sesquiterpenes were oxidized in the JPAC reaction chamber, nano-CN formation was only observed during the UV-on periods. This indicates that the terpene oxidation products formed during the dark periods (primarily by ozonolysis) either did not have the right properties or were not abundant enough to form, activate and/or grow nano-CN to sizes above the detection limit of the PSM-CPC setup.

## **4.2 Simulations of the observed new particle formation events**

The first simulations were designed in order to constrain the VOC wall losses and the mechanisms responsible for the observed particle growth (Sect 4.2.1 and Sect 4.2.2). For these simulations, we used a fixed nano-CN formation ratio of  $20 \text{ cm}^{-3} \text{ s}^{-1}$  during the UV-light on periods, except for the first 12 minutes with UV-light on for which we used  $J = 80 \text{ cm}^{-3} \text{ s}^{-1}$ , for Day-1 and Day-2 and  $60 \text{ cm}^{-3} \text{ s}^{-1}$  for Day-3. During the UV-light off periods the nano-CN formation rate was zero. The nano-CN had a dry diameter of 1.5 nm and was assumed to be composed of equal number of sulphuric acid and  $\text{ELVOC}_{\text{nuc1}}$  molecules. After, constraining the VOC wall losses and the potential particle growth mechanisms, we investigated several nano-CN formation mechanisms (Eq. 1-6) and compared the results against the results from the simulations with a fixed nano-CN formation rate (Sect. 4.2.3).

### **4.2.1 Modelling the reversible VOC wall deposition**

Figure 6a shows the modelled total particle volume concentration (PV) starting 14 days prior to the start of the intensive experimental campaign. The measured PV during the campaign is also displayed. The model results are from a simulation with the 2D-VBS. Figure 6b and c illustrate how the 2D-VBS compounds with different  $C^*$  were distributed onto the glass walls and the PTFE Teflon floor, respectively. The LVOCs ( $C_{298}^* < 10^{-1} \mu\text{g m}^{-3}$ ) deposited both onto the glass and Teflon surfaces, while the SVOCs ( $C_{298}^* > 10^{-1} \mu\text{g m}^{-3}$ ) were exclusively found at the Teflon floor where they could absorb into  $C_w$ . Some of the compounds with  $C_{298}^* = 10^{-1} \mu\text{g m}^{-3}$  deposited onto the glass walls shortly after the UV-light was turned on, but when the

condensation sink was increased and when the terpene inflow concentration into the reaction chamber was lowered (Day 2-4), the gas-phase concentrations of these compounds never reached above their pure liquid saturation concentrations, so they evaporated from the glass walls. Figure S9 in the supplementary material shows similar results but for a simulation where the MCMv3.2 compounds and additional ELVOCs (R1) were used to represent the condensable organic compounds.

Figure 7 shows the 2D-VBS VOC composition for: (a) the SOA particles, (b) the gas-phase, (c) the VOCs on the glass walls and (d) the VOCs on the PTEF Teflon floor, at Day-3 and after 5 hours with UV-lights on. The bar at  $O:C = 1$ ,  $\log_{10} C_{298}^* = -7$  corresponds to the ELVOCs which were assumed to be formed from ozonolysis and OH-oxidation of monoterpenes and sesquiterpenes (molar yield of 7 % and 1 %, respectively). After 16.5 days of continuous experiments,  $1.4 \text{ mg m}^{-3}$  of SVOCs had deposited onto the PTEF Teflon floor according to the model simulations. The largest fraction of the wall deposited VOCs were first generation terpene oxidation products ( $O:C=0.4$ ). A fraction of these SVOCs can re-evaporated and reacted with OH in the gas-phase. This explains why the modelled SOA formation was gradually increasing during the first 15 days (Fig. 6a), although all the other model conditions were identical. A similar pattern in the modelled SOA particle volume was also observed when the SOA formation was simulated with the MCM compounds (Fig. S8a). The ELVOCs (that are formed as first generation oxidation products (R1)) and the LVOCs (formed from OH-oxidation of the first generation oxidation products), primarily deposited onto the glass walls. However, in total the VOCs deposited onto the glass walls only made up 5 % of the total amount of VOCs on the chamber walls.

We also performed simulations assuming that the JPAC reaction chamber walls behave as FEP Teflon walls (Eq. 8), in which case  $k_e = 4.2 \text{ s}^{-1}$  and the  $a_w$  parameterization was taken from Zhang et al. (2014). For compounds with a molar mass of  $300 \text{ g mol}^{-1}$  and vapour pressures in the range  $10^{-2}$  to  $10^{-10} \text{ Pa}$  the  $k_{w,i}$  varies from  $2 \times 10^{-5}$  to  $7 \times 10^{-4} \text{ s}^{-1}$ . Thus, for these model simulations the ELVOC wall losses were about 15 times lower than what was observed by Ehn et al. (2014). Fig. S9 compares the measured total particle volume concentration with the modelled total particle volume concentration from a simulation with this wall loss parameterization. With the lower VOC wall losses, the model overestimated the SOA formation by a factor of 2-3 and there was no gradual increase in the SOA formation due to re-evaporation of SVOCs from the walls during the days before the intensive measurement

campaign started.

#### 4.2.2 Evaluation of potential particle growth mechanisms

When using the 2D-VBS, the modelled SOA composition was dominated by LVOCs and SVOCs formed from second- and multi-generation OH-oxidation products. This was the case even if we considered that ELVOCs were formed as first generation products after the O<sub>3</sub>- and OH-oxidation of monoterpenes and sesquiterpenes (Fig. 7a). The reason for this is the large ELVOC wall losses in the JPAC chamber and the small condensation sink during the new-particle formation events. During the UV-light on periods, the gas-phase 2D-VBS VOC composition was dominated by oxidized SVOCs formed by fragmentation of the first generation oxidation products (Fig. 7b).

In Fig. 8 we compare the modelled (a) total particle number concentration and (b) total particle volume concentration with the observations from the PSM-CPC and the SMPS. The model results are from simulations with the 2D-VBS with or without ELVOC formation from ozonolysis and OH-oxidation of all monoterpenes and sesquiterpenes (molar yield of 7 % and 1 %, respectively), as well as from a simulation where the condensable organic compounds were represented by the MCMv3.2 compounds (in total 488 compounds with  $p_0 < 10^{-2}$  Pa, including ELVOCs from ozonolysis of  $\alpha$ -pinene and  $\Delta^3$ -carene). For this simulation we also considered rapid peroxyhemiacetal dimer formation in the particle phase using Eq. 7 and  $B = 200 \text{ M}^{-1} \text{ s}^{-1}$ . Without consideration of this type of a rapid acid catalysed dimer formation process, the particle growth was substantially underestimated and almost no SOA was formed when we simulated the SOA formation using the MCM compounds (Fig. S8a). Shown are also the results from a simulation with only one non-volatile condensable organic compound. In the model, this compound was formed as a first generation oxidation product from O<sub>3</sub> and OH oxidation of all monoterpenes and sesquiterpenes with a mass yield of 60 % (molar yield of 25 %). Figure 9 shows results from the same simulations as in Fig 8, but here we instead compare the estimated SOA particle mass yields from the model with those derived from the measurements. Both in the model and for the measurements the SOA particle density was assumed to be  $1400 \text{ kg m}^{-3}$ . The SOA mass yields were estimated by dividing the total SOA particle mass with the amount of reacted terpenes (not including isoprene). The amount of reacted terpenes was estimated as the difference between the in and outflow terpene concentrations.

For all model simulations, the model overestimated the SOA particle volume formation and

SOA mass yield during Day-1 but tended to underestimate or give similar values as the measurements for Day 2-4. The most likely explanation to this is that the BVOC composition was substantially different during Day-1 (ocimene which reacts rapidly with  $O_3$  may not form SOA in the same extent as e.g.  $\alpha$ -pinene). The best agreement between the model and measured particle volume concentration was found with the 2D-VBS method ( $R^2 = 0.836$  with ELVOCs formation and  $R^2 = 0.835$  without ELVOC formation). For the simulation with the non-volatile one product model,  $R^2 = 0.796$ , and for the simulation with MCMv3.2 and acid catalysed PHA dimer formation,  $R^2 = 0.820$ .

Figure S10 in the supplementary material compares the modelled total particle volume concentrations from simulations with  $B = 10$  or  $200$ , or using a constant PHA dimer formation rate of  $12 \text{ M}^{-1} \text{ s}^{-1}$  based on the work by Shiraiwa et al. (2013). With  $B = 10$  the modelled PV are in very good agreement with the measured PV for Day-1 but for the following days the model substantially underestimated the PV. With a constant PHA dimer formation rate of  $12 \text{ M}^{-1} \text{ s}^{-1}$  the model gives 3 times higher PV than the measurements for Day-1 but gives reasonable PV formation for Day 2-4.

Figure 10 shows the modelled SOA volatility distribution as a function of particle size. The results are from a simulation with the 2D-VBS, including ELVOC formation from monoterpenes and sesquiterpens oxidized by  $O_3$  and OH. As expected, the smallest particles contained the largest mole fraction of ELVOCs because of the Kelvin effect.

Figure 11 shows the modelled and measured particle number size distributions at  $\frac{1}{2}$ , 1, 2 and 5 hours of UV-lights on, for each day of the experimental campaign. The model results are from a simulation with the 2D-VBS including ELVOC formation from monoterpenes and sesquiterpenes oxidized by  $O_3$  and OH. For Day-1, the model overestimated the particle growth rate, which can also be seen from the overestimated SOA formation (Fig. 8b). For the remainder of the experimental campaign, the modelled particle number size distributions were in good agreement with the SMPS measurements, except for the particles having a diameter  $< 30 \text{ nm}$ , for which where the model gave substantially higher concentrations. A contributing explanation for this feature can be non-accounted diffusion losses of particles in the SMPS inlet.

In the supplementary we show how the volatility distribution of the MCM compounds and the SOA formation changed when the  $NO_x$  concentration in the inflow to the chamber was changed in the range  $0.05$  to  $1 \text{ ppbv}$  (Fig. S11). When the  $NO_x$  concentration was increased to

from 0.05 to 1 ppbv the particle SOA volume concentration was increased slightly (~10 %).

### 4.2.3 Evaluation of potential nano-CN formation mechanisms

In this section we evaluate the different nano-CN formation mechanisms described in Sect 3.2. For these simulations we used the 2D-VBS to simulate the evolution of the condensable organic compounds. Because the exact vapour pressures, formation mechanisms and concentrations of ELVOCs still are very uncertain, we cannot dismiss the possibility that the new particle formation (formation of particles with  $D_p > 1.6$  nm) was limited by the activation of nano-CN and not by the nano-CN formation rate itself. In this section we evaluate possible nano-CN formation mechanism with the assumption that it was the nano-CN formation that primarily limited the observed new particle formation during the experiments.

Table 3 gives the coefficient of determination ( $R^2$ ) between the modelled total particle number concentration and the measured total particle number concentration ( $D_p > 1.6$  nm) from the PSM-CPC setup, and for the nano-CN mechanisms (parameterizations) that gave a  $R^2 > 0.85$ . The best agreement ( $R^2 > 0.97$ ) between the modelled and measured total particle number concentration was achieved with a nano-CN formation mechanism that involves both  $H_2SO_4$  and ELVOCs formed from OH-oxidation or OH and  $O_3$  oxidation of monoterpenes and sesquiterpenes (Eq. 3) or from Eq. 4 if the  $ELVOC_{nuc}$  molecules exclusively were formed from ozonolysis of sesquiterpenes. These are the only mechanisms for which  $R^2$  were higher than with a fixed nano-CN formation rate during the UV-light on periods.

In Fig. 12 we compare the modelled total particle number concentration when calculating  $J$  using Eq. 1, 2 and 3. With Eq. 3, the  $ELVOC_{nuc}$  were either assumed to be formed from ozonolysis and OH-oxidation of monoterpenes and sesquiterpenes or only from OH-oxidation. Displayed are also the results from simulations with constant  $J = 20 \text{ cm}^{-3} \text{ s}^{-1}$  during the UV-light on periods and  $J = 0 \text{ cm}^{-3} \text{ s}^{-1}$  during the UV-light of periods.

## 5 Summary and conclusion

In this study, we used the ADCHAM model to simulate the nano-CN formation and growth during an experimental campaign in the Jülich Plant Atmosphere Chamber, which focused on new particle formation induced by photochemical reactions of VOCs emitted from real plants (Dal Maso et al., 2014). With the model we evaluated potential nano-CN formation and

growth mechanisms and how the VOC chamber wall losses influenced the SOA formation and composition.

Chamber wall losses can have a profound influence on the SOA formation. In this work we showed that the contribution of ELVOCs to the nano-CN formation and growth was effectively suppressed due to their rapid and irreversible wall losses. Thus, it is questionable whether this type of smog chamber experiments is ideal for the evaluation of possible mechanisms responsible for the observed new particle formation in the atmosphere.

In the lack of ELVOCs, one possible mechanism that can explain the initial particle growth is rapid heterogeneous dimer formation of SVOCs. In this work, we found out that acid catalysed peroxyhemiacetal formation between aldehydes and hydroperoxides may explain the observed particle growth. However, the particle growth could be modelled equally well if the SOA was formed by condensation of low-volatility second- and multi-generation OH gas-phase oxidation products simulated with a 2D-VBS approach. Thus, based on our model simulations, we cannot conclude whether the observed particle growth primarily was driven by low-volatility organic compounds formed in the gas-phase or by rapid dimer formation in the particle phase. However, without the later mechanism the model fails to reproduce the observed SOA formation when using the MCMv3.2 oxidation products as condensable organic compounds.

Our results suggest that  $\text{H}_2\text{SO}_4$  is one of the key compounds involved in the new particle formation, but cannot solely explain the new particle formation process. During the simulated experiments, the best agreement between the modelled and measured total particle number concentration was achieved when using a nano-CN formation rate of the form  $J = K[\text{H}_2\text{SO}_4][\text{ELVOC}_{\text{nucI}}]$ .

## Acknowledgements

P. Roldin would like to thank the Cryosphere-Atmosphere Interactions in a Changing Arctic Climate (CRAICC) and the Swedish Research Council for Environment, Agricultural Sciences and Spatial Planning FORMAS (Project No. 214-2014-1445) for financial support. L. Liao wishes to thank the Maj and Tor Nessling foundation for financial support (grant No 2009362), as well as the Academy of Finland (project No. 128731). D. Mogensen would like to thank the doctoral program in Atmospheric Sciences (ATM-DP) at the University of Helsinki for financial support. We would like to acknowledge HENVI (Helsinki University



Centre for Environment), The FCoE (The Centre of Excellence in Atmospheric Science – From Molecular and Biological processes to the Global Climate (ATM)), the strategic research area MERGE (Modelling the Regional and Global Earth system) and the PEGASOS (Pan-European Gas-Aerosolsclimate interaction Study, project No FP7-ENV-2010-265148) project. We would also like to thank Prof. Gordon McFiggans' research group at the University of Manchester, and especially Dr. David Topping, for helpful discussions and for providing the Python script (now a publicly available function called Comp-SysProp: <http://ratty.cas.manchester.ac.uk/informatics/>) to calculate Nannoolal-based sub-cooled liquid saturation vapour pressures for all organic compounds included in this paper.

## References

- Almeida, J., Schobesberger, S., Kürten, A., Ortega, I. K., Kupiainen-Määttä, O., Praplan, A. P., Adamov, A., Amorim, A., Bianchi, F., and Breitenlechner, M.: Molecular understanding of sulphuric acid-amine particle nucleation in the atmosphere, *Nature*, 502, 359–363, 2013.
- Berndt, T., Stratmann, F., Sipilä, M., Vanhanen, J., Petäjä, T., Mikkilä, J., Grüner, A., Spindler, G., Lee Mauldin III, R., Curtius, J., Kulmala, M., and Heintzenberg, J.: Laboratory study on new particle formation from the reaction OH+SO<sub>2</sub>: influence of experimental conditions, H<sub>2</sub>O vapour, NH<sub>3</sub> and the amine tert-butylamine on the overall process, *Atmos. Chem. Phys.*, 10, 7101–7116, doi:10.5194/acp-10-7101-2010, 2010.
- Bonn, B. and Moortgat, G. K.: Sesquiterpene ozonolysis: origin of atmospheric new particle formation from biogenic hydrocarbons, *Geophys. Res. Lett.*, 30, 1585, doi:10.1029/2003GL017000, 2003.
- Boy, M., Rannik, Ü., Lehtinen, K. E. J., Tarvainen, V., Hakola, H., and Kulmala, M.: Nucleation events in the continental boundary layer: long-term statistical analyses of aerosol relevant characteristics, *J. Geophys. Res.*, 108, 4667, doi:10.1029/2003JD003838, 2003.
- Boy, M., Mogensen, D., Smolander, S., Zhou, L., Nieminen, T., Paasonen, P., Plass-Dülmer, C., Sipilä, M., Petäjä, T., Mauldin, L., Berresheim, H., and Kulmala, M.: Oxidation of SO<sub>2</sub> by stabilized Criegee intermediate (sCI) radicals as a crucial source for atmospheric sulfuric acid concentrations, *Atmos. Chem. Phys.*, 13, 3865–3879, doi:10.5194/acp-13-3865-2013, 2013.
- Claeys, M., Graham, B., Vas, G., Wang, W., Vermeylen, R., Pashynska, V., Cafmeyer, J.,

1 Guyon, P., Andreae, M. O., Artaxo, P., and Maenhaut, W.: Formation of secondary organic  
2 aerosols through photooxidation of isoprene, *Science*, 303, 1173–1176, 2004. 27975 Crump,  
3 J. G. and Seinfeld, J. H.: Turbulent deposition and gravitational sedimentation of an aerosol in  
4 a vessel of arbitrary shape, *J. Aerosol Sci.*, 12, 405–415, 1981.

5 Dal Maso, M., Liao, L., Wildt, J., Kiendler-Scharr, A., Kleist, E., Tillmann, R., Sipilä, M.,  
6 Hakala, J., Lehtipalo, K., Ehn, M., Kerminen, V.-M., Kulmala, M., Worsnop, D., and  
7 Mentel, T.: A chamber study of the influence of boreal BVOC emissions and sulphuric acid  
8 on nanoparticle formation rates at ambient concentrations, *Atmos. Chem. Phys. Discuss.*, 14,  
9 31319–31360, doi:10.5194/acpd-14-31319-2014, 2014.

10 Damian, V., Sandu, A., Damian, M., Potra, F., and Carmichael, G. R.: The kinetic  
11 preprocessor KPP-a software environment for solving chemical kinetics, *Comput. Chem.*  
12 *Eng.*, 26, 1567–1579, 2002.

13 Donahue, N. M., Epstein, S. A., Pandis, S. N., and Robinson, A. L.: A two-dimensional  
14 volatility basis set: 1. organic-aerosol mixing thermodynamics, *Atmos. Chem. Phys.*, 11,  
15 3303–3318, doi:10.5194/acp-11-3303-2011, 2011.

16 Ehn, M., Thornton, J. A., Kleist, E., Sipilä, M., Junninen, H., Pullinen, I., Springer, M.,  
17 Rubach, F., Tillmann, R., Lee, B., Lopez-Hilfiker, F., Andres, S., Acir, I.-H., Rissanen, M.,  
18 Jokinen, T., Schobesberger, S., Kangasluoma, J., Kontkanen, J., Nieminen, T., Kurtén, T.,  
19 Nielsen, L. B., Jorgensen, S., Kjaergaard, H. G., Canagaratna, M., Maso, M. D., Berndt, T.,  
20 Petäjä, T., Wahner, A., Kerminen, V.-M., Kulmala, M., Worsnop, D. R., Wildt, J., and  
21 Mentel, T. F.: A large source of low volatility secondary organic aerosol, *Nature*, 506, 476–  
22 479, 2014.

23 Epstein, S., Riipinen, I., and Donahue, N. M.: A Semiempirical Correlation between Enthalpy  
24 of Vaporization and Saturation Concentration for Organic Aerosol, *Environ. Sci. Technol.*,  
25 44, 743–748, 2010.

26 Guenther, A., Hewitt, C. N., Erickson, D., Fall, R., Geron, C., Graedel, T., Harley, P.,  
27 Klinger, L., Lerdau, M., McKay, W. A., Pierce, T., Scholes, B., Steinbrecher, R., Tallamraju,  
28 R., Taylor, J., and Zimmerman, P.: A global-model of natural volatile organic-compound  
29 emissions, *J. Geophys. Res.*, 100, 8873–8892, doi:10.1029/94JD02950, 1995.

30 Hallquist, M., Wenger, J. C., Baltensperger, U., Rudich, Y., Simpson, D., Claeys, M.,  
31 Dommen, J., Donahue, N. M., George, C., Goldstein, A. H., Hamilton, J. F., Herrmann, H.,

1 Hoffmann, T., Iinuma, Y., Jang, M., Jenkin, M. E., Jimenez, J. L., Kiendler-Scharr, A.,  
2 Maenhaut, W., McFiggans, G., Mentel, Th. F., Monod, A., Prévôt, A. S. H., Seinfeld, J. H.,  
3 Surratt, J. D., Szmigielski, R., and Wildt, J.: The formation, properties and impact of  
4 secondary organic aerosol: current and emerging issues, *Atmos. Chem. Phys.*, 9, 5155–5236,  
5 doi:10.5194/acp-9-5155-2009, 2009.

6 Hao, L. Q., Yli-Pirilä, P., Tiitta, P., Romakkaniemi, S., Vaattovaara, P., Kajos, M. K., Rinne,  
7 J., Heijari, J., Kortelainen, A., Miettinen, P., Kroll, J. H., Holopainen, J. K., Smith, J. N.,  
8 Joutsensaari, J., Kulmala, M., Worsnop, D. R., and Laaksonen, A.: New particle formation  
9 from the oxidation of direct emissions of pine seedlings, *Atmos. Chem. Phys.*, 9, 8121–8137,  
10 doi:10.5194/acp-9-8121-2009, 2009.

11 Heiden, A. C., Kobel, K., Langebartels, C., Schuh-Thomas, G., and Wildt, J.: Emissions of  
12 oxygenated volatile organic compounds from plants – Part I: Emissions from lipoxygenase  
13 activity, *J. Atmos. Chem.*, 45, 143–172, 2003.

14 Hermansson, E., Roldin, P., Rusanen, A., Mogensen, D., Kivekäs, N., Väänänen, R., Boy, M.,  
15 and Swietlicki, E.: Biogenic SOA formation through gas-phase oxidation and gas-to-particle  
16 partitioning – a comparison between process models of varying complexity, *Atmos. Chem.*  
17 *Phys.*, 14, 11853–11869, doi:10.5194/acp-14-11853-2014, 2014.

18 Hoffmann, T., Odum, J. R., Bowman, F., Collins, D., Klockow, D., Flagan, R. C., and  
19 Seinfeld, J. H.: Formation of organic aerosols from the oxidation of biogenic hydrocarbons, *J.*  
20 *Atmos. Chem.*, 26, 189–222, 1997.

21 Hoffmann, T., Bandur, R., Marggraf, U., and Linscheid, M.: Molecular composition of  
22 organic aerosols formed in the  $\alpha$ -pinene/O<sub>3</sub> reaction: implications for new particle formation  
23 processes, *J. Geophys. Res.*, 103, 25569–25578, 1998.

24 Jacobson, M. Z.: Numerical techniques to solve condensational and dissolutional growth  
25 equations when growth is coupled to reversible aqueous reactions, *Aerosol Sci. Technol.*, 27,  
26 491–498, 1997.

27 Jacobson, M. Z.: A Solution to the Problem of Nonequilibrium Acid/Base Gas-Particle  
28 Transfer at Long Time Step, *Aerosol Sci. Technol.*, 39, 92–103, 2005.

29 Jenkin, M. E., Saunders, S. M., and Pilling, M. J.: The tropospheric degradation of volatile  
30 organic compounds: a protocol for mechanism development, *Atmos. Environ.*, 31, 81–104,  
31 1997.

1 Jenkin, M. E., Wyche, K. P., Evans, C. J., Carr, T., Monks, P. S., Alfarra, M. R., Barley, M.  
 2 H., McFiggans, G. B., Young, J. C., and Rickard, A. R.: Development and chamber  
 3 evaluation of the MCM v3.2 degradation scheme for  $\beta$ -caryophyllene, *Atmos. Chem. Phys.*,  
 4 12, 5275–5308, doi:10.5194/acp-12-5275-2012, 2012.

5 Jimenez, J. L., Canagaratna, M. R., Donahue, N. M., Prevot, A. S. H., Zhang, Q., Kroll, J. H.,  
 6 DeCarlo, P. F., Allan, J. D., Coe, H., Ng, N. L., Aiken, A. C., Docherty, K. S., Ulbrich, I. M.,  
 7 Grieshop, A. P., Robinson, A. L., Duplissy, J., Smith, J. D., Wilson, K. R., Lanz, V. A.,  
 8 Hueglin, C., Sun, Y. L., Tian, J., Laaksonen, A., Raatikainen, T., Rautiainen, J., Vaattovaara,  
 9 P., Ehn, M., Kulmala, M., Tomlinson, J. M., Collins, D. R., Cubison, M. J., Dunlea, E. J.,  
 10 Huffman, J. A., Onasch, T. B., Alfarra, M. R., Williams, P. I., Bower, K., Kondo, Y.,  
 11 Schneider, J., Drewnick, F., Borrmann, S., Weimer, S., Demerjian, K., Salcedo, D., Cottrell,  
 12 L., Griffin, R., Takami, A., Miyoshi, T., Hatakeyama, S., Shimono, A., Sun, J. Y., Zhang, Y.  
 13 M., Dzepina, K., Kimmel, J. R., Sueper, D., Jayne, J. T., Herndon, S. C., Trimborn, A. M.,  
 14 Williams, L. R., Wood, E. C., Middlebrook, A. M., Kolb, C. E., Baltensperger, U., and  
 15 Worsnop, D. R.: Evolution of Organic Aerosols in the Atmosphere, *Science*, 326, 1525–1529,  
 16 2009.

17 Kerminen, V.-M., Petäjä, T., Manninen, H. E., Paasonen, P., Nieminen, T., Sipilä, M.,  
 18 Junninen, H., Ehn, M., Gagné, S., Laakso, L., Riipinen, I., Vehkamäki, H., Kurten, T., Ortega,  
 19 I. K., Dal Maso, M., Brus, D., Hyvärinen, A., Lihavainen, H., Leppä, J., Lehtinen, K. E. J.,  
 20 Mirme, A., Mirme, S., Hörrak, U., Berndt, T., Stratmann, F., Birmili, W., Wiedensohler, A.,  
 21 Metzger, A., Dommen, J., 5 Baltensperger, U., Kiendler-Scharr, A., Mentel, T. F., Wildt, J.,  
 22 Winkler, P. M., Wagner, P. E., Petzold, A., Minikin, A., Plass-Dülmer, C., Pöschl, U.,  
 23 Laaksonen, A., and Kulmala, M.: Atmospheric nucleation: highlights of the EUCAARI  
 24 project and future directions, *Atmos. Chem. Phys.*, 10, 10829–10848, doi:10.5194/acp-10-  
 25 10829-2010, 2010.

26 Kiendler-Scharr, A., Wildt, J., Dal Maso, M., Hohaus, T., Kleist, E., Mentel, T. F., Tillmann,  
 27 R., Uerlings, R., Schurr, U., and Wahner, A.: New particle formation in forests inhibited by  
 28 isoprene emissions, *Nature*, 461, 381–384, 2009.

29 Kokkola, H., Yli-Pirilä, P., Vesterinen, M., Korhonen, H., Keskinen, H., Romakkaniemi, S.,  
 30 Hao, L., Kortelainen, A., Joutsensaari, J., Worsnop, D. R., Virtanen, A., and Lehtinen, K. E. J.:  
 31 The role of low volatile organics on secondary organic aerosol formation, *Atmos. Chem.*  
 32 *Phys.*, 14, 1689–1700, doi:10.5194/acp-14-1689-2014, 2014.

1 Korhonen, H., Lehtinen, K. E. J., and Kulmala, M.: Multicomponent aerosol dynamics model  
 2 UHMA: model development and validation, *Atmos. Chem. Phys.*, 4, 757–771,  
 3 doi:10.5194/acp-4-757-2004, 2004.

4 Kulmala, M., Pirjola, U., and Makela, J. M.: Stable sulphate clusters as a source of new  
 5 atmospheric particles, *Nature*, 404, 66–69, 2000.

6 Kulmala, M., Vehkamäki, H., Petäjä, T., Dal Maso, M., Lauri, A., Kerminen, V. M., Birmili,  
 7 W., and McMurry, P. H.: Formation and growth rates of ultrafine atmospheric particles: a  
 8 review of observations, *J. Aerosol Sci.*, 35, 143–176, 2004.

9 Kulmala, M., Lehtinen, K. E. J., and Laaksonen, A.: Cluster activation theory as an  
 10 explanation of the linear dependence between formation rate of 3nm particles and sulphuric  
 11 acid concentration, *Atmos. Chem. Phys.*, 6, 787–793, doi:10.5194/acp-6-787-2006, 2006.

12 Kulmala, M., Riipinen, I., Sipilä, M., Manninen, H. E., Petäjä, T., Junninen, H., Dal Maso,  
 13 M., Mordas, G., Mirme, A., Vana, M., Hirsikko, A., Laakso, L., Harrison, R. M., Hanson, I.,  
 14 Leung, C., Lehtinen, K. E. J., and Kerminen, V. M.: Toward direct measurement of  
 15 atmospheric nucleation, *Science*, 318, 89–92, 2007.

16 Kulmala, M., Nieminen, T., Chellapermal, R., Makkonen, R., Bäck, J., and Kerminen, V.-M.:  
 17 Climate feedbacks linking the increasing atmospheric CO<sub>2</sub> concentration, BVOC emissions,  
 18 aerosols and clouds in forest ecosystems, in: *Biology, Controls and Models of Tree Volatile*  
 19 *Organic Compound Emissions*, Springer, Springer Netherlands, 489–508, 2013.

20 Kulmala, M., Nieminen, T., Nikandrova, A., Lehtipalo, K., Manninen, H. E., Kajos, M. K.,  
 21 Kolari, P., Lauri, A., Petäjä, T., Krejci, R., Hansson, H.-C., Swietlicki, E., Lindroth, A.,  
 22 Christensen, T. R., Arneth, A., Hari, P., Bäck, J., Vesala, T., and Kerminen, V.-M.: CO<sub>2</sub> –  
 23 induced terrestrial climate feedback mechanism: from carbon sink to aerosol source and back,  
 24 *Boreal Environ. Res.*, 19, 122–131, 2014.

25 Kurtén, T., Loukonen, V., Vehkamäki, H., and Kulmala, M.: Amines are likely to enhance  
 26 neutral and ion-induced sulfuric acid-water nucleation in the atmosphere more effectively  
 27 than ammonia, *Atmos. Chem. Phys.*, 8, 4095–4103, doi:10.5194/acp-8-4095-2008, 2008.

28 Laaksonen, A., Kulmala, M., O’Dowd, C. D., Joutsensaari, J., Vaattovaara, P., Mikkonen, S.,  
 29 Lehtinen, K. E. J., Sogacheva, L., Dal Maso, M., Aalto, P., Petäjä, T., Sogachev, A., Yoon, Y.  
 30 J., Lihavainen, H., Nilsson, D., Facchini, M. C., Cavalli, F., Fuzzi, S., Hoffmann, T., Arnold,  
 31 F., Hanke, M., Sellegri, K., Umann, B., Junkermann, W., Coe, H., Allan, J. D., Alfarra, M. R.,

1 Worsnop, D. R., Riekkola, M. -L., Hyötyläinen, T., and Viisanen, Y.: The role of VOC  
 2 oxidation products in continental new particle formation, *Atmos. Chem. Phys.*, 8, 2657–2665,  
 3 doi:10.5194/acp-8-2657-2008, 2008.

4 Lai, A. and Nazaroff, W. W.: Modelling indoor particle deposition from turbulent flow onto  
 5 smooth surfaces, *J. Aerosol Sci.*, 31, 463–476, 2000.

6 Matsunaga, A. and Ziemann, P. J.: Gas-wall partitioning of organic compounds in a Teflon  
 7 film chamber and potential effects on reaction product and aerosol yield measurements,  
 8 *Aerosol Sci. Tech.*, 44, 881–892, 2010.

9 Mauldin, R., Frost, G., Chen, G., Tanner, D., Prevot, A., Davis, D., and Eisele, F.: OH  
 10 measurements during the First Aerosol Characterization Experiment (ACE 1): observations  
 11 and model comparisons, *J. Geophys. Res.*, 103, 16713–16729, doi:10.1029/98JD00882, 1998.

12 McMurry, P. H., and Friedlander, S. K.: New particle formation in the presence of an aerosol,  
 13 *Atmos. Environ.*, 13, 1635–1651, 1979.

14 McMurry P. H., and Grosjean, D.: Gas and aerosol wall losses in Teflon film smog chambers,  
 15 *Environ. Sci. Technol.* 19, 1176–1182, 1985.

16 McMurry, P. H. and Rader, D. J.: Aerosol wall losses in electrically charged chambers.  
 17 *Aerosol Sci. Technol.*, 4, 249–268, 1985.

18 McMurry P. H., Kulmala, M., Worsnop D. R.: Special Issue on Aerosol Measurements in the  
 19 1 nm Range, *Aerosol Sci. Technol.* 45, i, 2011.

20 Mentel, T. F., Wildt, J., Kiendler-Scharr, A., Kleist, E., Tillmann, R., Dal Maso, M., Fisseha,  
 21 R., Hohaus, Th., Spahn, H., Uerlings, R., Wegener, R., Griffiths, P. T., Dinar, E., Rudich, Y.,  
 22 and Wahner, A.: Photochemical production of aerosols from real plant emissions, *Atmos.*  
 23 *Chem. Phys.*, 9, 4387–4406, doi:10.5194/acp-9-4387-2009, 2009.

24 Metzger, A., Verheggen, B., Dommen, J., Duplissy, J., Prevot, A. S., Weingartner, E.,  
 25 Riipinen, I., Kulmala, M., Spracklen, D. V., Carslaw, K. S., and Baltensperger U.: Evidence  
 26 for the role of organics in aerosol particle formation under atmospheric conditions, *P. Natl.*  
 27 *Acad. Sci. USA*, 107, 6646–6651, 2010.

28 Mirme, S., Mirme, A., Minikin, A., Petzold, A., Hörrak, U., Kerminen, V. -M., and Kulmala,  
 29 M.: Atmospheric sub-3 nm particles at high altitudes, *Atmos. Chem. Phys.*, 10, 437–451,  
 30 doi:10.5194/acp-10-437-2010, 2010.

1 Nannoolal, Y., Rarey, J., Ramjugernath, D., and Cordes, W.: Estimation of pure component  
2 properties Part 1, Estimation of the normal boiling point of non-electrolyte organic  
3 compounds via group contributions and group interactions, *Fluid Phase Equilibr.*, 226, 45–63,  
4 2004.

5 Nannoolal, J., Rarey, J., and Ramjugernath, D.: Estimation of pure component properties Part  
6 3. Estimation of the vapour pressure of non-electrolyte organic compounds via group  
7 contributions and group interactions *Fluid Phase Equilibria*, 269, 117–133, 2008.

8 Owen, S. M., Harley, P., Guenther, A., and Hewitt, C. N.: Light dependency of VOC  
9 emissions from selected Mediterranean plant species, *Atmos. Environ.*, 36, 3147–3159, 2002.

10 Paasonen, P., Nieminen, T., Asmi, E., Manninen, H. E., Petäjä, T., Plass-Dülmer, C., Flentje,  
11 H., Birmili, W., Wiedensohler, A., Hörrak, U., Metzger, A., Hamed, A., Laaksonen, A.,  
12 Facchini, M. C., Kerminen, V.-M., and Kulmala, M.: On the roles of sulphuric acid and low-  
13 volatility organic vapours in the initial steps of atmospheric new particle formation, *Atmos.*  
14 *Chem. Phys.*, 10, 11223–11242, doi:10.5194/acp-10-11223-2010, 2010.

15 Park, S. H., Kim, H. O., Han, Y. T., Kwon, S. B., and Lee, K. W.: Wall loss rate of  
16 polydispersed aerosols, *Aerosol Sci. Tech.*, 35, 710–717, 2001.

17 Petäjä, T., Mauldin, III, R. L., Kosciuch, E., McGrath, J., Nieminen, T., Paasonen, P., Boy,  
18 M., Adamov, A., Kotiaho, T., and Kulmala, M.: Sulfuric acid and OH concentrations in a  
19 boreal forest site, *Atmos. Chem. Phys.*, 9, 7435–7448, doi:10.5194/acp-9-7435-2009, 2009.

20 Pierce, J. R., Engelhart, G. J., Hildebrandt, L., Weitkamp, E. A., Pathak, R. K., Donahue, N.  
21 M., Robinson, A. L., Adams, P. J., and Pandis, S. N.: Constraining Particle Evolution from  
22 Wall Losses, Coagulation, and Condensation-Evaporation in Smog- Chamber Experiments:  
23 Optimal Estimation Based on Size Distribution Measurements, *Aerosol Sci. Technol.*, 42,  
24 1001–1015, 2008.

25 Riccobono, F., Schobesberger, S., Scott, C. E., Dommen, J., Ortega, I. K., Rondo, L.,  
26 Almeida, J. a., Amorim, A., Bianchi, F., Breitenlechner, M., David, A., Downard, A., Dunne,  
27 E. M., Duplissy, J., Ehrhart, S., Flagan, R. C., Franchin, A., Hansel, A., Junninen, H., Kajos,  
28 M., Keskinen, H., Kupc, A., Kürten, A., Kvashin, A. N., Laaksonen, A., Lehtipalo, K.,  
29 Makhmutov, V., Mathot, S., Nieminen, T., Onnela, A., Petäjä, T., Praplan, A. P., Santos, F.  
30 D., Schallhart, S., Seinfeld, J. H., Sipilä, M., Spracklen, D. V., Stozhkov, Y., Stratmann, F.,  
31 Tomé, A., Tsagkogeorgas, G., Vaattovaara, P., Viisanen, Y., Virtala, A., Wagner, P. E.,

1 Weingartner, E., Wex, H., Wimmer, D., Carslaw, K. S., Curtius, J., Donahue, N. M., Kirkby,  
2 J., Kulmala, M., Worsnop, D. R., and Baltensperger, U.: Oxidation products of biogenic  
3 emissions contribute to nucleation of atmospheric particles, *Science*, 344, 717–721, 2014.

4 Riipinen, I., Sihto, S.-L., Kulmala, M., Arnold, F., Dal Maso, M., Birmili, W., Saarnio, K.,  
5 Teinilä, K., Kerminen, V.-M., Laaksonen, A., and Lehtinen, K. E. J.: Connections between  
6 atmospheric sulphuric acid and new particle formation during QUEST III–IV campaigns in  
7 Heidelberg and Hyytiälä, *Atmos. Chem. Phys.*, 7, 1899–1914, doi:10.5194/acp-7-1899-2007,  
8 2007.

9 Riipinen, I., Pierce, J. R., Donahue, N. M., and Pandis, S. N.: Equilibration time scales of  
10 organic aerosol inside thermodenuders: Evaporation kinetics versus thermodynamics, *Atmos.*  
11 *Environ.*, 44, 597–607, 2010.

12 Riipinen, I., Yli-Juuti, T., Pierce, J. R., Petäjä, T., Worsnop, D. R., Kulmala, M., and  
13 Donahue, N. M.: The contribution of organics to atmospheric nanoparticle growth, *Nat.*  
14 *Geosci.*, 5, 453–458, 2012.

15 Roldin, P., Swietlicki, E., Schurgers, G., Arneth, A., Lehtinen, K. E. J., Boy, M., and  
16 Kulmala, M.: Development and evaluation of the aerosol dynamics and gas phase chemistry  
17 model ADCHEM, *Atmos. Chem. Phys.*, 11, 5867–5896, doi:10.5194/acp-11-5867- 2011,  
18 2011.

19 Roldin, P., Eriksson, A. C., Nordin, E. Z., Hermansson, E., Mogensen, D., Rusanen, A., Boy,  
20 M., Swietlicki, E., Svenningsson, B., Zelenyuk, A., and Pagels, J.: Modelling non-equilibrium  
21 secondary organic aerosol formation and evaporation with the aerosol dynamics, gas and  
22 particle-phase chemistry kinetic multilayer model ADCHAM, *Atmos. Chem. Phys.*, 14,  
23 7953–7993, doi:10.5194/acp-14-7953-2014, 2014.

24 Ruuskanen, T. M., Taipale, R., Rinne, J., Kajos, M. K., Hakola, H., and Kulmala, M.:  
25 Quantitative long-term measurements of VOC concentrations by PTR-MS: annual cycle at a  
26 boreal forest site, *Atmos. Chem. Phys. Discuss.*, 9, 81–134, doi:10.5194/acpd-9-81-2009,  
27 2009.

28 Saunders, S. M., Jenkin, M. E., Derwent, R. G., and Pilling, M. J.: Protocol for the  
29 development of the Master Chemical Mechanism, MCM v3 (Part A): tropospheric  
30 degradation of nonaromatic volatile organic compounds, *Atmos. Chem. Phys.*, 3, 161–180,  
31 doi:10.5194/acp-3-161-2003, 2003.



1 Schimang, R., Folkers, A., Kleffmann, J., Kleist, E., Miebach, M., and Wildt, J.: Uptake of  
2 gaseous nitrous acid (HONO) by several plant species, *Atmos. Environ.*, 40, 1324–1335,  
3 2006.

4 Schobesberger, S., Junninen, H., Bianchi, F., Lönn, G., Ehn, M., Lehtipalo, K., Dommen, J.,  
5 Ehrhart, S., Ortega, I. K., Franchin, A., Nieminen, T., Riccobono, F., Hutterli, M., Duplissy,  
6 J., Almeida, J., Amorim, A., Breitenlechner, M., Downard, A. J., Dunne, E. M., Flagan, R. C.,  
7 Kajos, M., Keskinen, H., Kirkby, J., Kupc, A., Kürten, A., Kurtén, T., Laaksonen, A., Mathot,  
8 S., Onnela, A., Praplan, A. P., Rondo, L., Santos, F. D., Schallhart, S., Schnitzhofer, R.,  
9 Sipilä, M., Tomé, A., Tsagkogeorgas, G., Vehkamäki, H., Wimmer, D., Baltensperger, U.,  
10 Carslaw, K. S., Curtius, J., Hansel, A., Petäjä, T., Kulmala, M., Donahue, N. M., and  
11 Worsnop, D. R.: Molecular understanding of atmospheric particle formation from sulfuric  
12 acid and large oxidized organic molecules, *P. Natl. Acad. Sci. USA*, 110, 17223–17228, 2013.

13 Sihto, S.-L., Kulmala, M., Kerminen, V.-M., Dal Maso, M., Petäjä, T., Riipinen, I., Korhonen,  
14 H., Arnold, F., Janson, R., Boy, M., Laaksonen, A., and Lehtinen, K. E. J.: Atmospheric  
15 sulphuric acid and aerosol formation: implications from atmospheric measurements for  
16 nucleation and early growth mechanisms, *Atmos. Chem. Phys.*, 6, 4079–4091,  
17 doi:10.5194/acp-6-4079-2006, 2006.

18 Sipilä, M., Berndt, T., Petäjä, T., Brus, D., Vanhanen, J., Stratmann, F., Patokoski, J.,  
19 Mauldin, Roy, L. I., Hyvarinen, A.-P., Lihavainen, H., and Kulmala, M.: The role of sulfuric  
20 acid in atmospheric nucleation, *Science*, 327, 1243–1246, 2010.

21 Spracklen, D. V., Jimenez, J. L., Carslaw, K. S., Worsnop, D. R., Evans, M. J., Mann, G. W.,  
22 Zhang, Q., Canagaratna, M. R., Allan, J., Coe, H., McFiggans, G., Rap, A., and Forster, P.:  
23 Aerosol mass spectrometer constraint on the global secondary organic aerosol budget, *Atmos.*  
24 *Chem. Phys.*, 11, 12109–12136, doi:10.5194/acp-11-12109-2011, 2011.

25 Surratt, J. D., Murphy, S. M., Kroll, J. H., Ng, N. L., Hildebrandt, L., Sorooshian, A.,  
26 Szmigielski, R., Vermeulen, R., Maenhaut, W., Claeys, M., Flagan, R. C., and Seinfeld, J. H.:  
27 Chemical composition of secondary organic aerosol formed from the photooxidation of  
28 isoprene, *J. Phys. Chem. A*, 110, 9665–9690, 2006.

29 Topping, D. O., McFiggans, G. B., Kiss, G., Varga, Z., Facchini, M. C., Decesari, S., and  
30 Mircea, M.: Surface tensions of multi-component mixed inorganic/organic aqueous systems  
31 of atmospheric significance: measurements, model predictions and importance for cloud

1 activation predictions, *Atmos. Chem. Phys.*, 7, 2371–2398, doi:10.5194/acp-7-2371-2007,  
2 2007.

3 Tsigaridis, K. and Kanakidou, M.: Global modelling of secondary organic aerosol in the  
4 troposphere: a sensitivity analysis, *Atmos. Chem. Phys.*, 3, 1849–1869, doi:10.5194/acp-3-  
5 1849-2003, 2003.

6 Vanhanen, J., Mikkilä, J., Lehtipalo, K., Sipilä, M., Manninen, H. E., Siivola, E., Petäjä, T.,  
7 and Kulmala, M.: Particle size magnifier for nano-CN detection, *Aerosol Sci. Tech.*, 45, 533–  
8 542, 2011.

9 VanReken, T. M., Greenberg, J. P., Harley, P. C., Guenther, A. B., and Smith, J. N.: Direct  
10 measurement of particle formation and growth from the oxidation of biogenic emissions,  
11 *Atmos. Chem. Phys.*, 6, 4403–4413, doi:10.5194/acp-6-4403-2006, 2006.

12 Wang, Z. B., Hu, M., Mogensen, D., Yue, D. L., Zheng, J., Zhang, R. Y., Liu, Y., Yuan, B.,  
13 Li, X., Shao, M., Zhou, L., Wu, Z. J., Wiedensohler, A., and Boy, M.: The simulations of  
14 sulfuric acid concentration and new particle formation in an urban atmosphere in China,  
15 *Atmos. Chem. Phys.*, 13, 11157–11167, doi:10.5194/acp-13-11157-2013, 2013.

16 Zhang, R.: Getting to the critical nucleus of aerosol formation, *Science*, 328, 1366–1367,  
17 2010.

18 Zhang, X., Cappa, C. D., Jathar, S. H., McVay, R. C., Ensberg, J. J., Kleeman, M. J., and  
19 Seinfeld, J. H.: Influence of vapor wall loss in laboratory chambers on yields of secondary  
20 organic aerosol, *P. Natl. Acad. Sci. USA*, 111, 5802–5807, 2014.

21 Zhang, X., Schwantes, R. H., McVay, R. C., Lignell, H., Coggon, M. M., Flagan, R. C., and  
22 Seinfeld, J. H.: Vapor wall deposition in Teflon chambers, *Atmos. Chem. Phys.*, 15, 4197-  
23 4214, doi:10.5194/acp-15-4197-2015, 2015.

24 Zuend, A., Marcolli, C., Luo, B. P., and Peter, T.: A thermodynamic model of mixed organic-  
25 inorganic aerosols to predict activity coefficients, *Atmos. Chem. Phys.*, 8, 4559–4593,  
26 doi:10.5194/acp-8-4559-2008, 2008.

27 Zuend, A., Marcolli C., Booth, A. M., Lienhard, D. M., Soonsin, V., Krieger, U. K., Topping,  
28 D. O., McFiggans G., Peter, T., and Seinfeld, J. H.: New and extended parameterization of the  
29 thermodynamic model AIOMFAC: calculation of activity coefficients for organic-inorganic  
30 mixtures containing carboxyl, hydroxyl, carbonyl, ether, ester, alkenyl, alkyl, and aromatic

functional groups, Atmos. Chem. Phys., 11, 9155–9206, doi:10.5194/acp-11-9155-2011, 2011.

Table 1. The VOCs measured with GC-MS in the JPAC plant chamber. The measured concentrations were used as input for the ADCHAM model. The “other MTs” and “other SQTs” refer to other monoterpenes and sesquiterpenes than those specified in the table, respectively.

Isoprene				
$\alpha$ -pinene	$\beta$ -pinene	myrcene	sabinene	camphene
ocimene	$\Delta^3$ -carene	$\alpha$ -terpinene	$\Delta$ -terpinene	$\alpha$ -phellandrene
$\beta$ -phellandrene	terpinolene	tricyclene	other MTs	
farnesene	$\beta$ -caryophyllene	$\alpha$ -longipinene	$\Delta$ -cardinene	other SQTs
2-butanol	hexanal	benzene	toluene	eucalyptol
nonanal	bornyl acetate	methyl salicylate		

Table 2. Summary of the model sensitivity tests that we performed in order to evaluate and constrain possible mechanisms for the formation and growth of nano-CN during the JPAC experiments.

<b>Condensable VOC properties method</b>	MCMv3.2 + the Nannoolal vapour pressure method	2D-VBS
<b>2D-VBS assumptions</b>	Functionalization, fragmentation and OH reaction rates	O:C of the first generation products
<b>Particle dry deposition loss rates</b>	Varying $u^*$ in the range 0.1-0.01 m s <sup>-1</sup>	
<b>Gas-phase chemistry</b>	Uncertainties related to the assumed NO <sub>x</sub> inflow concentration	Influence of the UV-light on the VOC composition
<b>Influence of ELVOCs on the particle growth</b>	ELVOC formation from ozonolysis and OH-oxidation of terpenes	
<b>Nano-CN formation and initial growth</b>	Mechanisms (Eq. 1-6)	Surface tension 0.02-0.07 N m <sup>-1</sup>
<b>Oligomerization in the particle phase</b>	Peroxyhemiacetal formation, possibly acid catalysed by co-condensing H <sub>2</sub> SO <sub>4</sub> (Eq. 7)	
<b>Non-ideal mixing in the particle phase</b>	Activity coefficients from AIOMFAC	
<b>Reversible VOC wall losses</b>	With or without absorptive uptake on the glass walls.	
<b>SOA phase-state</b>	Liquid-like SOA	Solid-like SOA

- 1 Table 3. Coefficient of determination ( $R^2$ ) between the modelled and measured (PSM-CPC)
- 2 total particle number concentration during the experimental campaign.

Nano-CN formation mechanism	ELVOC <sub>nucl</sub> source	$R^2$
Constant $J = 20 \text{ cm}^{-3} \text{ s}^{-1}$ when UV is on		0.968
H <sub>2</sub> SO <sub>4</sub> activation (Eq. 1)		0.942
H <sub>2</sub> SO <sub>4</sub> kinetic (Eq. 2)		0.887
H <sub>2</sub> SO <sub>4</sub> – ELVOC kinetic (Eq. 3)	MT and SQT ox. by O <sub>3</sub> and OH	0.975
H <sub>2</sub> SO <sub>4</sub> – ELVOC kinetic (Eq. 3)	MT and SQT ox. OH	0.977
H <sub>2</sub> SO <sub>4</sub> – ELVOC kinetic (Eq. 3)	SQT ox. by O <sub>3</sub> and OH	0.944
H <sub>2</sub> SO <sub>4</sub> – ELVOC (Eq. 4)	SQT ox. by O <sub>3</sub> and OH	0.959
H <sub>2</sub> SO <sub>4</sub> – ELVOC (Eq. 4)	SQT ox. by O <sub>3</sub>	0.975
ELVOC (Eq. 5)	MT and SQT ox. OH	0.903

3

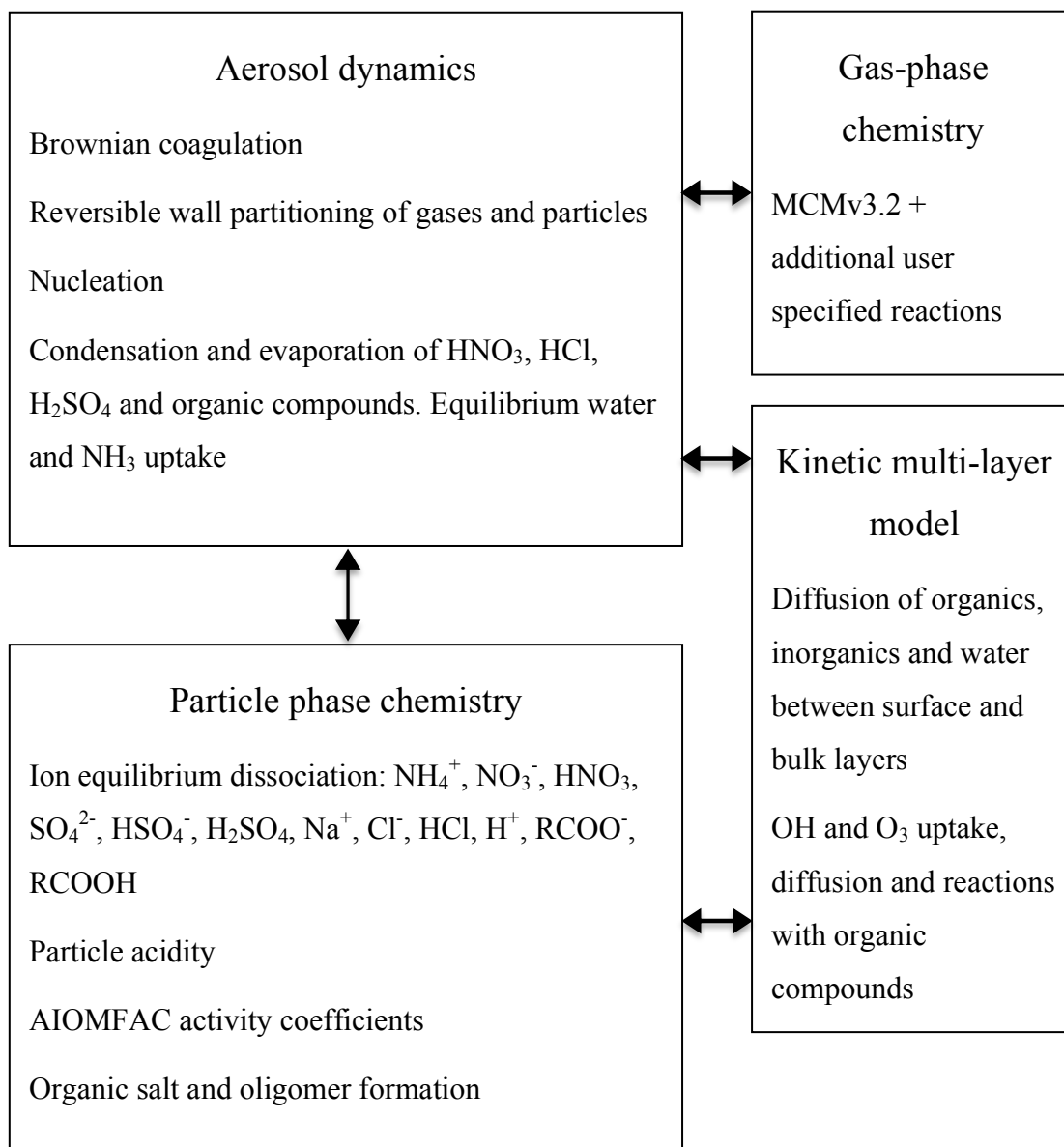
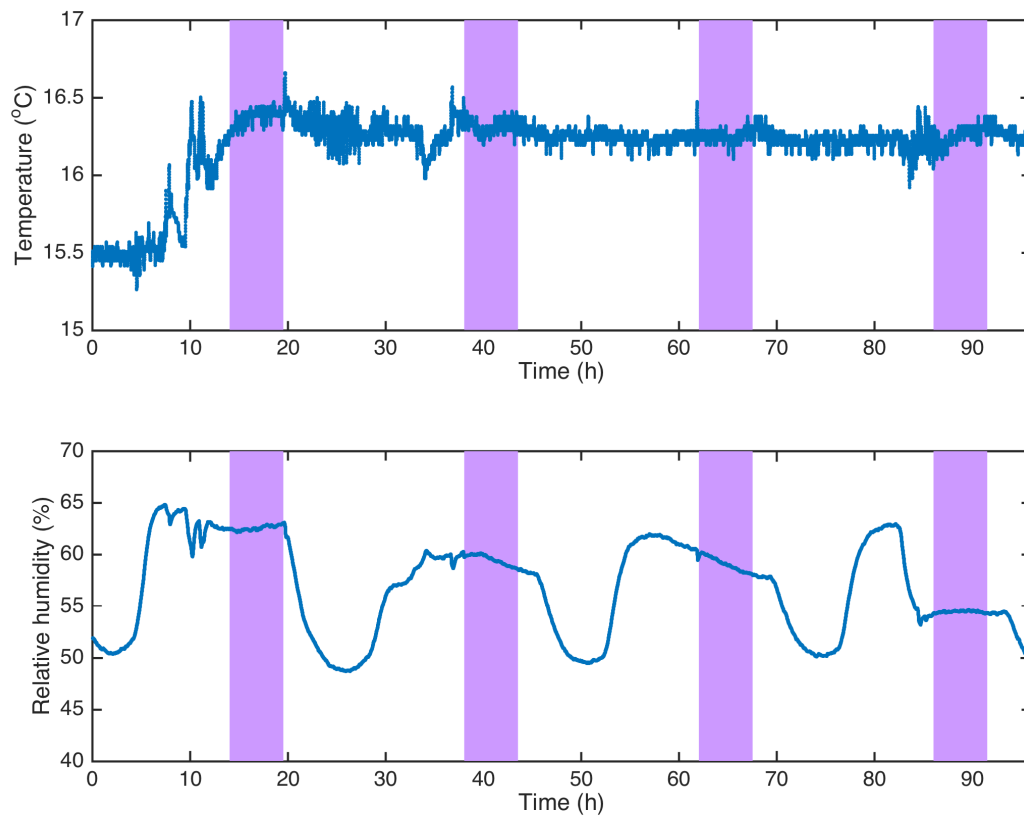


Figure 1. Schematic picture of the ADCHAM model structure.



1  
2 Figure 2. Measured temperature (a) and relative humidity (b) in the JPAC reaction chamber  
3 during the first four days of the measurement campaign. The purple bars indicate UV-on  
4 periods.

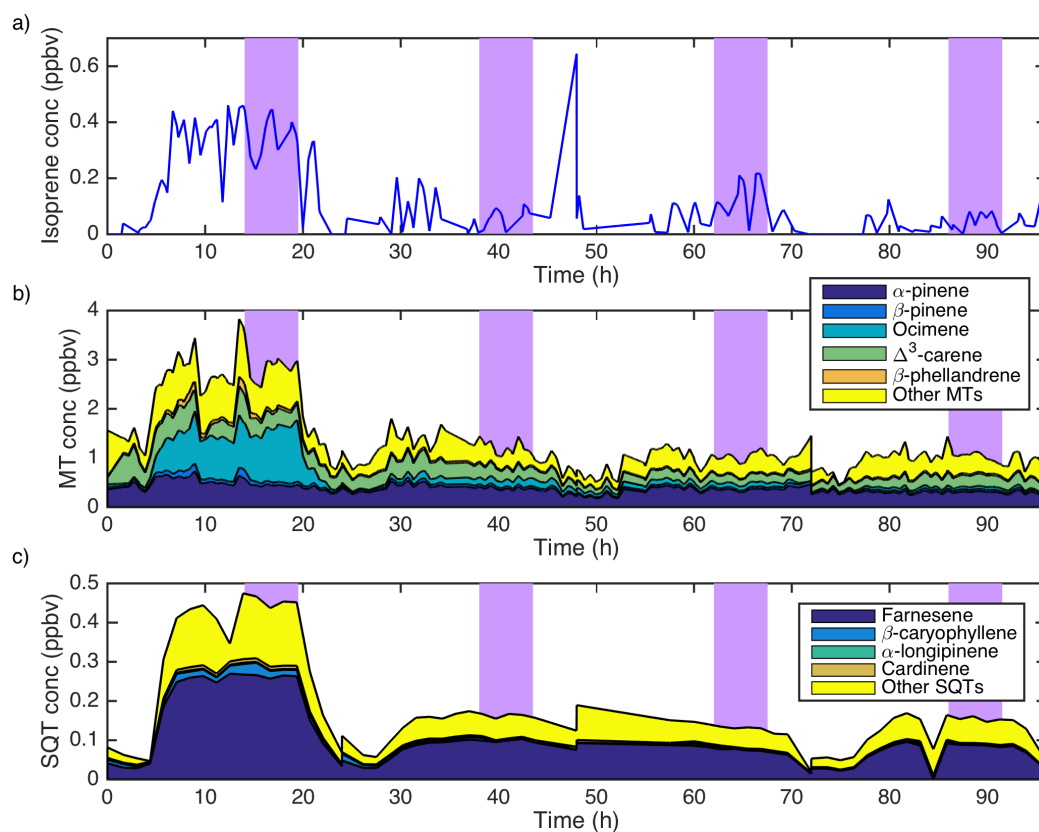
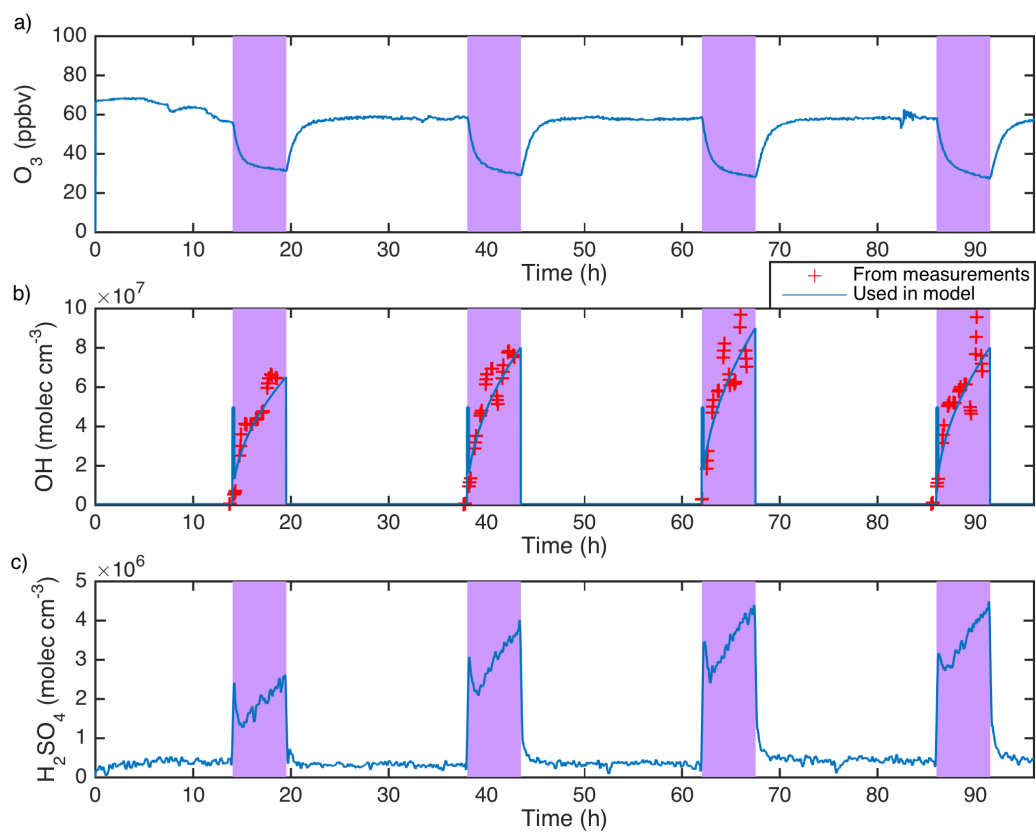


Figure 3. Isoprene (a), monoterpene (b) , and sesquiterpene (c) concentrations measured from the outlet air of the JPAC plant chamber. In Fig. b and c we left out those terpenes that had a negligible contribution to the total terpene concentration. Purple bars indicate UV-on periods during the measurements.





1  
2 Figure 4. (a) Measured  $O_3$  concentrations in the JPAC reaction chamber, (b) estimated OH  
3 concentration based on the observed 2-butanol loss rate and the OH concentration used as  
4 model input, and (c) measured  $H_2SO_4$  concentration.

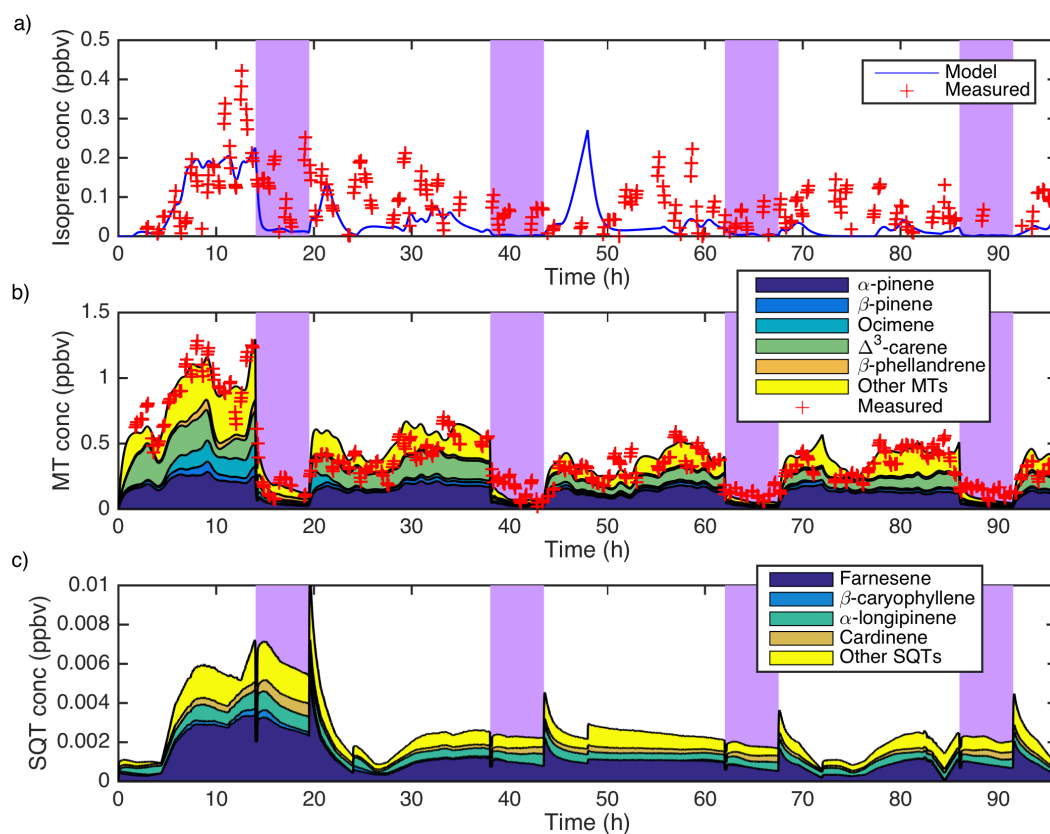


Figure 5. Modelled isoprene (a), monoterpene (b), and sesquiterpene (c) concentrations together with the measured isoprene and monoterpene concentrations in the JPAC reaction chamber. In Fig. b we left out those monoterpenes that had a negligible contribution to the total monoterpene concentration. The purple bars indicate UV-on periods during the measurements.

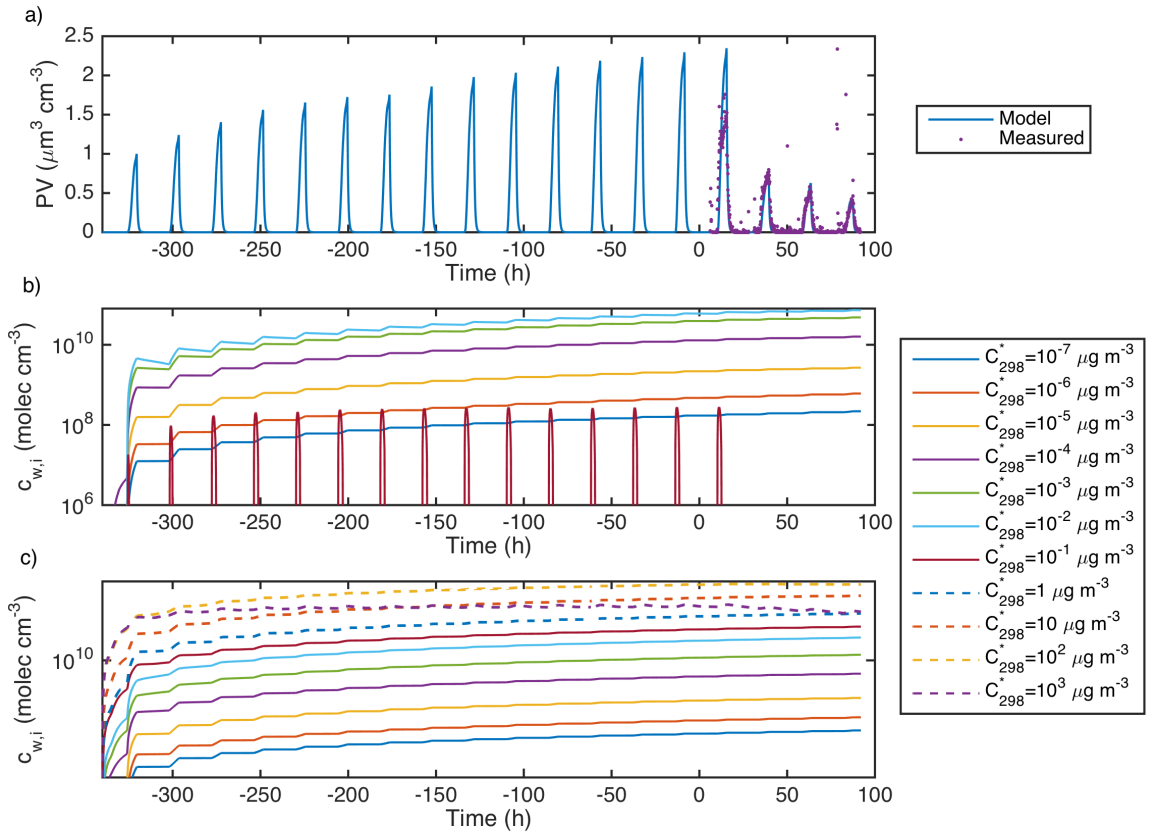
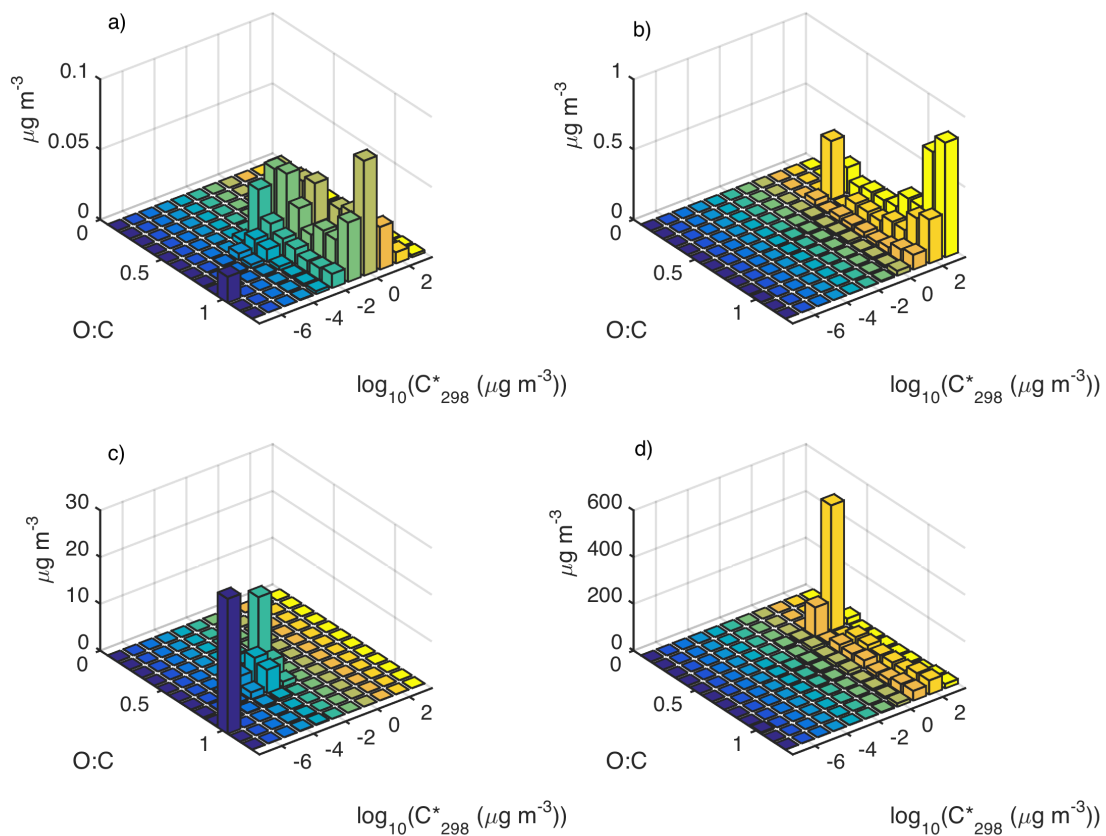


Figure 6. (a) Modelled and measured SOA volume formation and 2D-VBS VOC wall uptake onto (b) the glass walls and (c) the PTFE Teflon walls when considering that the PTFE Teflon walls behave as FEB Teflon walls (Eq. 8, 11 and 12). The VOCs are summed over the all O:C but divided into the different  $C_{298}^*$  bins in the 2D-VBS. At time 0 h the intensive measurement campaign started.



1  
2 Figure 7. Modelled 2D-VBS distribution for (a) the SOA particles, (b) the gas-phase, (c) the  
3 VOCs on the glass-walls and (d) the VOCs on the Teflon floor. The model results are from  
4 Day-3 after 5 hours with UV-lights on.

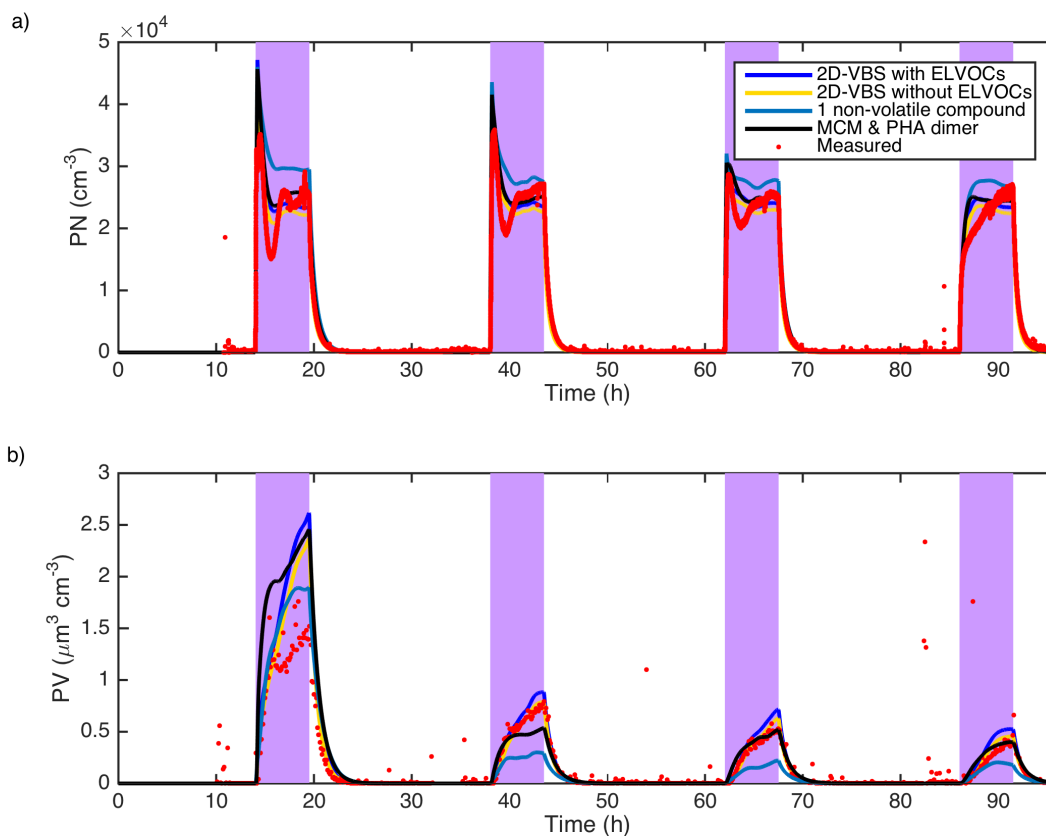


Figure 8. Modelled and measured (a) total particle number concentration and (b) total particle volume concentration. The model results are from simulations with the 2D-VBS and with or without ELVOC formation via ozonolysis and OH-oxidation of monoterpenes and sesquiterpenes, from a simulation when the MCM compounds were used as the condensable organic compounds and considering PHA dimer formation with Eq. 7, and from a simulation with only one condensable non-volatile compound. The mass yield of the non-volatile compound formed from  $O_3$  and OH oxidation of all monoterpenes and sesquiterpenes was 60 %.

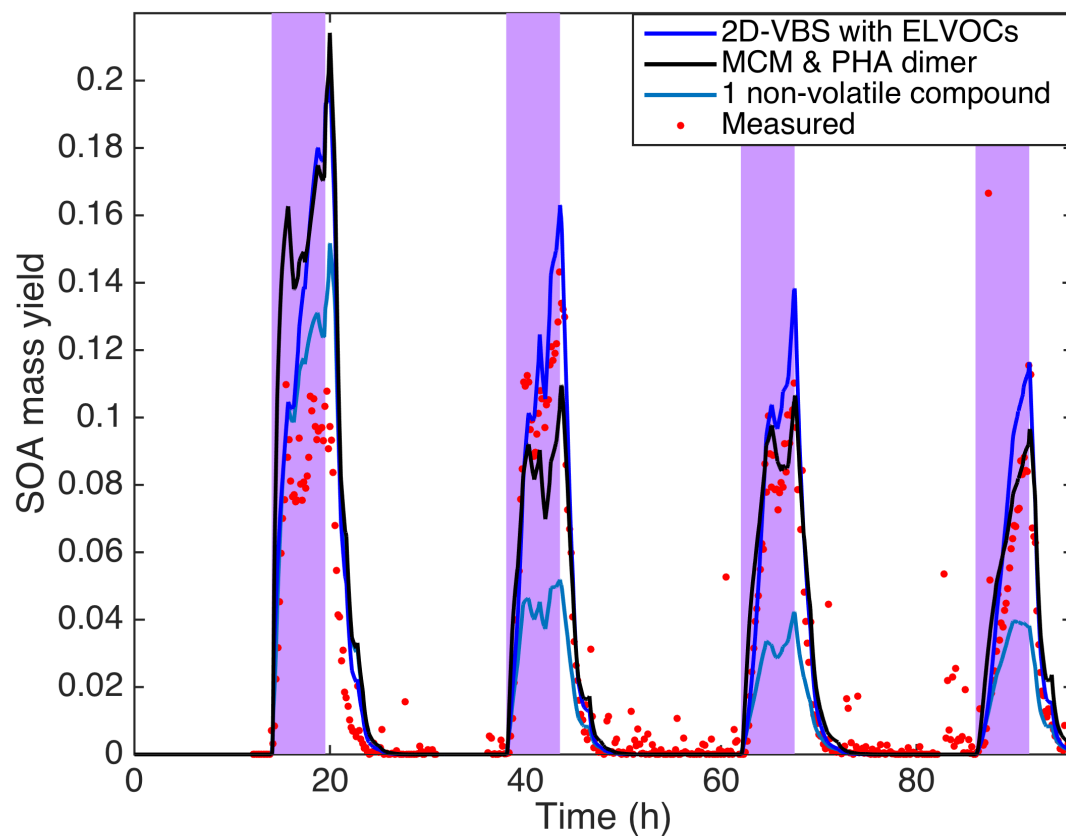


Figure 9. Modelled and measured SOA mass yields. The SOA density was assumed to be  $1400 \text{ kg m}^3$ .

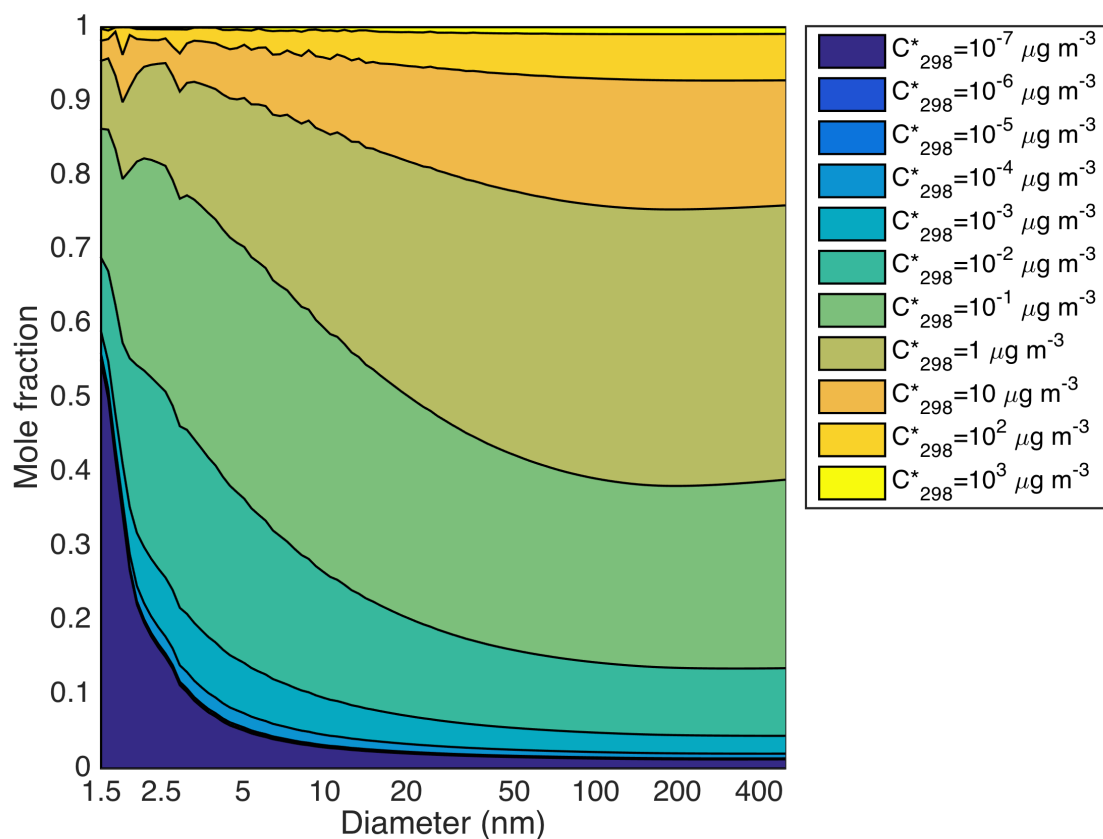


Figure 10. Modelled SOA volatility distribution as a function of the particle size from a simulation with the 2D-VBS and ELVOC formation from ozonolysis and OH-oxidation of monoterpenes and sesquiterpenes. The results are from Day-3 after 5 hours into the UV-light period.

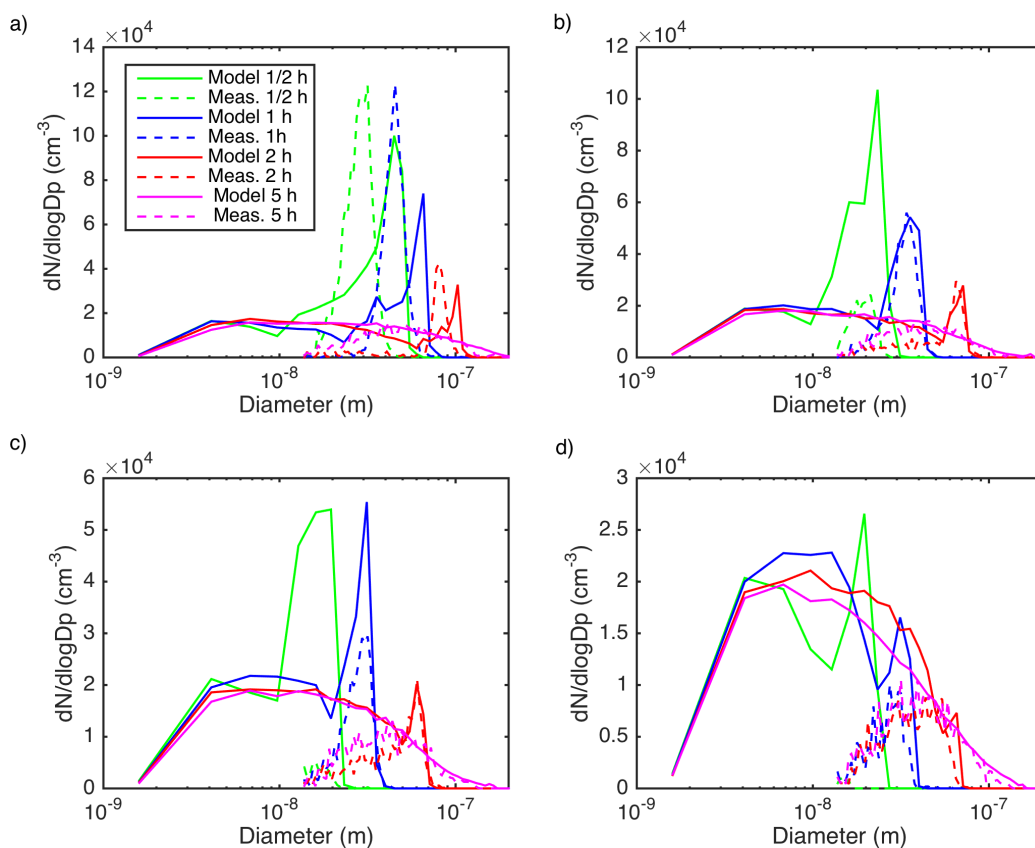


Figure 11. Modelled and measured particle number size distribution from (a) Day-1, (b) Day-2, (c) Day-3 and (d) Day-4 of the experimental campaign. The particle number size distributions are from ½, 1, 2 and 5 hours after the UV-light was turned on. The model results are from a simulation with the 2D-VBS (including ELVOC formation) and the full-moving size distribution method.



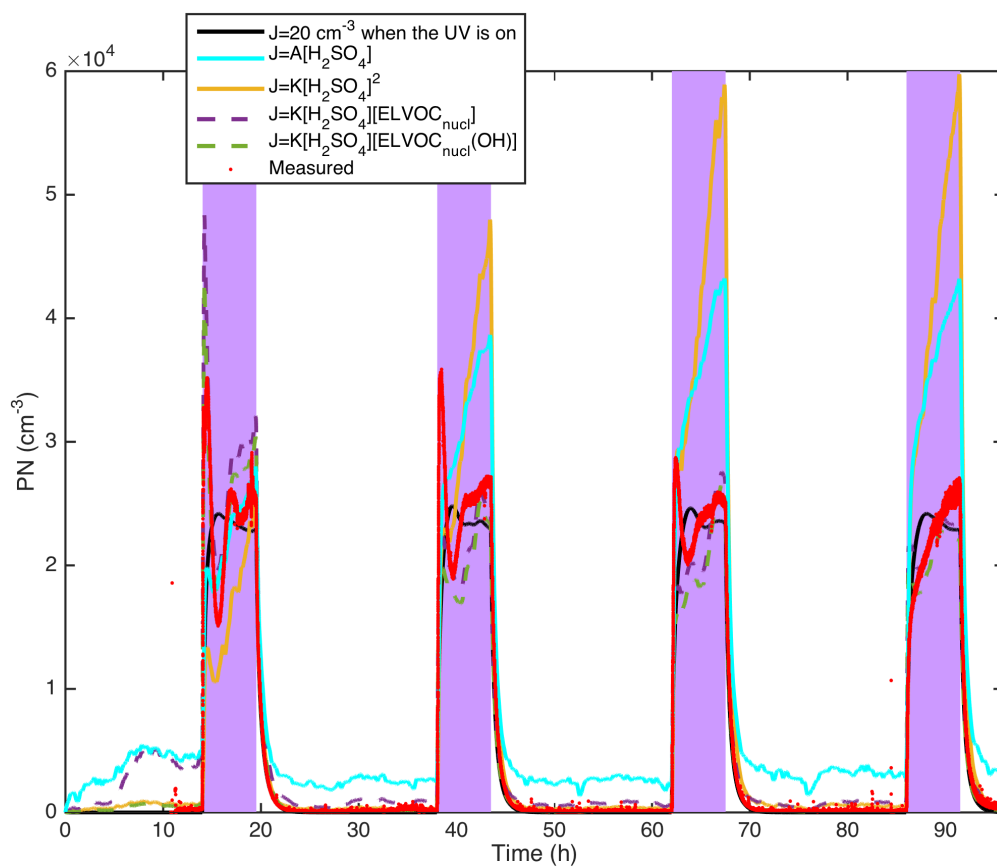


Figure 12. Measured (PSM-CPC) and modelled total particle number concentration with different nano-CN formation mechanism.